JOURNAL OF PROPULSION AND POWER
Vol. 32, No. 3, May-June 2016

Two-Time-Variable Perturbation Theory for Liquid-Rocket Combustion Instability

William A. Sirignano* and Jeremy Krieg†
University of California, Irvine, Irvine, California 92697

DOI: 10.2514/1.B35954

Nonlinear, transverse-mode, liquid-propellant-rocket-motor combustion instability is examined for the first time via a two-time-variable perturbation expansion in an amplitude parameter. Both triggered and spontaneous instability domains are studied. A specific coaxial multi-injector example demonstrates the matching process between wave dynamics and injection/combustion mechanisms. The combustion has a characteristic time for mixing, producing a time lag in the energy release rate relative to pressure. The coupled combustion process and wave dynamics are calculated for the first tangential mode. Two first-order ordinary differential equations are developed and solved for the amplitude and phase angle in the slow time. Limit cycles and transient behaviors are resolved. Nonlinear triggering is predicted in certain operational domains; above a critical initial amplitude, the amplitude grows; otherwise, it decays with time. A linear representation of the combustion process suffices to balance nonlinear nozzle damping. This perturbation approach provides better physical understanding than a computational fluid dynamics approach and allows lower-cost computation to determine trends over the key parameter domains. Moving a higher fraction of the propellant flow away from the chamber center has a destabilizing effect on the tangential mode. A most stable Mach-number value is deduced. The reduction to two governing ordinary differential equations benefits future optimization and control analyses.

Nomenclature

A	=	pressure oscillation amplitude
A_e	=	cross-sectional area of nozzle entrance, m^2
A_t	=	cross-sectional area of nozzle throat, m^2
A^*	=	pressure oscillation limit cycle amplitude
a	=	speed of sound, m/s
B	=	nondimensional parameter defined in Eq. (10)
c_p	=	specific heat at constant pressure, J/(kg · K)
c_v	=	specific heat at constant volume, J/(kg · K)
D	=	mass diffusivity, m^2/s
E	=	energy release rate per unit volume, $J/(m^3 \cdot s)$
E_1	=	complex coefficient for energy release rate used in Eq. (75)
$E_{c,1}$	=	energy-release-rate coefficient defined in Eq. (22), $J/(m^3 \cdot s)$
$E_{s,1}$	=	energy-release-rate coefficient defined in Eq. (24), $J/(m^3 \cdot s)$
f	=	frequency, s^{-1}
G	=	Green's function
h	=	specific enthalpy, J/kg
k_1-k_4	=	perturbation parameters defined in Eq. (59)
J_n	=	Bessel function of first kind and nth order
L	=	chamber length, m
L_f	=	flame length, m
M	=	Mach number
$\dot{M}$	=	steady-state injector mass flow rate
$\dot{m}$	=	mass flow rate, kg/s
N	=	number of injectors
P	=	complex coefficient for pressure used in Eq. (75)
p	=	pressure, $N\,m^{-2}$
Q	=	energy value per mass of fuel, J/kg
$Q_n(r)$	=	functions defined in Appendix A
$q_n(r)$	=	functions defined in Appendix A
R	=	chamber radius, m
R_s	=	mixture specific gas constant, J/(kg · K)
R_f	=	flame radius, m
R_i	=	inner radius of coaxial jet, m
R_o	=	outer radius of coaxial jet, m
r	=	radial position, m
s_{nh}	=	hth root for zero slope of Bessel function of first kind and order n
T	=	temperature, K
t	=	time, s
U	=	coaxial jet velocity, m/s
$\boldsymbol{u}$	=	vector velocity, m/s
u_j	=	Cartesian velocity component, m/s
u_r	=	radial velocity component, m/s
u_θ	=	tangential velocity component, m/s
$V_1(x)$	=	burning rate parameter defined by Sirignano and Krieg [27], m^{-1}
$V_2(x)$	=	integral quantity defined by Sirignano and Krieg [27]
$V_3(x)$	=	in-phase component of combustion response factor defined in Eq. (74)
$V_4(x)$	=	out-of-phase component of combustion response factor defined in Eq. (74)
W	=	Wronskian
x_j	=	Cartesian coordinate, m
Y_n	=	Bessel function of second kind and nth order
z	=	nondimensional fast time
$\Gamma(\gamma)$	=	function of gamma expanded in Eq. (15)
γ	=	ratio of specific heats
ε	=	nondimensional amplitude perturbation parameter
θ	=	azimuthal position
ν	=	fuel-to-oxygen mass stoichiometric ratio
ρ	=	density, $kg \cdot m^{-3}$
σ	=	small positive parameter characterizing slow time scale
τ	=	slow nondimensional time
τ_M	=	characteristic mixing time, s
ψ	=	phase angle
ω	=	angular frequency, rad/s
ω_2	=	limit cycle angular frequency perturbation, rad/s

Subscripts

F	=	fuel

Received 24 July 2015; revision received 16 October 2015; accepted for publication 18 October 2015; published online 11 January 2016.

*Professor, Department of Mechanical and Aerospace Engineering; sirignan@uci.edu. Fellow AIAA.

†Graduate Student Researcher, Department of Mechanical and Aerospace Engineering.

i = inflow condition
j = index for Cartesian coordinates
O = oxidizer
ss = steady state

I. Introduction

LIQUID-PROPELLANT-ROCKET-ENGINE (LPRE) combustion instability has been a longstanding natural phenomenon, which causes problems and creates the need for control. In a LPRE, the combustion process produces a very high-energy release rate per unit volume that, in many circumstances, has characteristic times that result in reinforcement of the acoustical oscillations and produces very high-pressure and -velocity amplitudes. These oscillations can cause undesirable oscillations in thrust, vibrations that result in problems for people or equipment on the spacecraft, and increased heat transfer in already critical regions, e.g., the nozzle throat. Transverse spinning waves can have substantially larger amplitudes than longitudinal waves because no shock waves form and thereby dissipation is reduced [1,2]. The combustion concentrates near the injector end, resulting in very high heat transfer rates to the injector. The increased heat transfer at the injector and/or nozzle throat often leads to the destruction of those walls and disaster for the flight mission.

Theoretical, computational, and experimental research has been underway at varying levels of intensity for more than a half century. Most of the physics of the nonlinear acoustic oscillations were identified in the 1950s and 1960s, but the knowledge of the details of coupling with the combustion processes has trailed. An excellent compilation of major research during that early period is provided by Harrje and Reardon [1]. Also, an interesting discussion of the famous F-1 Rocket Motor instability problems is given by Oefelein and Yang [3]. Two types of instability occur: linear (i.e., spontaneous) instability and nonlinear (i.e., triggered) instability. The describing terms pertain to initiation only; all instabilities of concern have nonlinear behavior once established. Linear instabilities grow in amplitude from the normal noise associated with the high-mass flow, multi-injector rocket chamber environment; theoretically, they grow from infinitesimal disturbances. Nonlinear instabilities require an initiating disturbance of magnitude greater than a required threshold before becoming unstable. With a disturbance below the threshold value, stability is exhibited. A disruption in propellant mass flow or a very large fluctuation caused by transient operation can provide the necessary trigger for nonlinear growth. In experiments, small explosives have triggered nonlinear instabilities.

Each resonant mode oscillation is a characteristic of the particular combustion chamber and convergent portion of the nozzle. These resonant mode oscillations and their well-approximated frequencies are predictable by linear theory [1,4–6]. The lowest frequency mode is identified as the fundamental mode, while the other modes are overtones. Only in special situations are the overtones also harmonics of the fundamental mode; that is, their frequencies are integer multiples of the fundamental frequency. For transverse modes, the harmonics are not predicted by linear theory. It is well known from the theory of nonlinear oscillations [7] that, for many mechanical systems, nonlinear resonance can involve any of several developments: the generation of harmonics superimposed on the basic resonant mode, the simultaneous excitement of other resonant modes by the transfer of energy among modes, and the transfer of energy to a subharmonic mode of which the frequency is lower than the basic mode and related arithmetically to two or more resonant modes (e.g., the difference between two resonant frequencies).

There are two general types of acoustical combustion instability: driven instability and self-excited instability, as noted by Culick [6]. He describes evidence in some solid-propellant rockets of the former (driven) type in which vortex shedding (a more organized noise) causes kinematic waves (i.e., waves carried with the moving gas) of vorticity or entropy to travel to some point where an acoustical reflection occurs. The reflected wave causes more vortex shedding after travelling back, and a cyclic character results. These driven instabilities do not rely on acoustical chamber resonance, and acoustical waves travelling one way (upstream) are the only type of consequence with kinematic waves only travelling downstream by the kinematic definition. These driven-instability amplitudes are much smaller in amplitude since the energy level is limited by the initiating energy that causes the upstream-travelling acoustic wave; essentially, the upstream acoustic wave is repeatedly (i.e., periodically) initiated. (On the contrary, resonant self-excited oscillations need only one initiation and then receive energy additions in a periodic fashion from the combustion process building up its amplitude.) These driven instabilities have also been observed in ramjet combustors but never in liquid rockets and will not be addressed here. Self-excited instabilities are the primary type relevant to liquid-propellant rockets, although they also appear elsewhere.

Based on experiment and development-test experience [1], three stability domains can exist: unconditionally stable operation in which the amplitude of any disturbance (large or small) decays in time to the steady-state operation; unconditionally unstable operation in which the amplitude of any disturbance (large or small) grows in time to a limit-cycle oscillation; and bistable operation in which the amplitude of any disturbance grows to a limit-cycle above a specific threshold but decays to the steady-state results for disturbances of a magnitude below the threshold. These self-excited instabilities are not limited in amplitude by the energy of the initiation action; they find the energy within their own "macro" (i.e., chamber or acoustic wavelength scale) behavior as the oscillations grows and develops. So, the instability becomes macrolevel although the initiation can be microlevel (at least one order of magnitude smaller than the chamber scale). Moderate (normal steady-state rumbling) noise might initiate the linear instability in certain operational domains, and large disruptive noise (e.g., an experimental bomb, a large operational change, a large but temporary rogue injector blockage, or the injector exit vortex) might trigger the nonlinear instability in some other operational domain. In those cases, noise or disruptions are typically only initiators with modest energy levels compared to the energy of the ultimate oscillation. Startup transients can also initiate instabilities so that a steady state never comes into existence. The instability is driven by a coupling between combustion and acoustics, not by the initiator. Certain relations between the resonant frequency and the characteristic times associated with the combustion process are required [2]. The limit-cycle amplitude of the oscillation is also related to certain parameters describing the combustion process. In situations in which triggering of an oscillation occurs, the threshold amplitude (or unstable limit-cycle amplitude) is related to certain combustion parameters.

A theoretical prediction of triggering was first given by Sirignano [8] for the longitudinal mode followed by Zinn [9] for the transverse mode. The approach predicts either a stable or unstable limit cycle for each point in the n, τ plane near the linear stability limit line. These early pioneering efforts on nonlinear triggering did not predict the expected higher-amplitude stable limit cycle in the n, τ domains where an unstable limit cycle and nonlinear triggering were predicted. Presumably, if the analyses were extended sufficiently beyond third-order terms in the amplitude parameter, the stable limit cycle would be determined.

Determination of the limit-cycle amplitude to lowest order of accuracy has involved linear combustion and nozzle flow terms matched against nonlinear gas dynamic terms for both cases with shocks and without shocks and for both longitudinal and transverse modes [2,8–10]. These linear terms are the lowest-order approximations to the forcing and damping of the oscillation. Nonlinear forcing and damping terms should appear to higher order. Of course, in computational fluid dynamics (CFD) computations at University of California, Irvine [11–15], the full nonlinear combustion and nozzle effects have been considered. In cases in which linear representation serves for a first approximation, the qualitative differences are small between the results using an ad hoc two-parameter combustion model [8,9,16,17] and the results using a physics-based description [10–15,18]; essentially, two parameters can do reasonably well describing the ratio of the energy-release-rate perturbation to the pressure perturbation to lowest order.

Culick [6] describes second-order and third-order perturbation analyses at California Institute of Technology [19–21] that never

predicted triggering action. This is not inconsistent with the previously described results that indicated that three types of stability zones could be predicted by any model that predicted the possibility of triggering. That is, by variation of operating parameters, some of the previous models [8,9,11,16] predicted a neighboring domain of unconditional stability and a neighboring domain of unconditional instability for any bistable domain where triggering occurred.

A complete review has not been attempted here. There are more detailed reviews of rocket-engine-combustion instability [1,4,6,22].

The goal of this study is to develop a model equation or small system of equations that describe the essential features of transverse nonlinear oscillations in cylindrical combustion chambers for LPREs. There is special interest in studying the nonlinear triggering phenomenon, using a first-principles description of the combustion process. It is important to keep in the model the terms that add energy and damp oscillations or produce a major change to the wave shape. The injected propellants is considered as preheated and gaseous; two-phase flows can be considered in the future.

II. Basic Equations for Wave Dynamics

The equations for the chamber wave dynamics will be simplified by assuming inviscid, non-heat-conducting, non-mass-diffusing flow. Turbulent fluctuations are considered small compared to acoustic amplitudes; also, the turbulent length scales are shorter than the acoustic wavelengths, which allows their neglect. The turbulence is generated largely by the jets of propellants entering the combustion chamber, and the length scales are determined by transverse jet dimensions and spacing between adjacent jets. In contrast, acoustic wavelengths are determined by the much larger chamber dimensions. Furthermore, kinematic waves with lengths substantially shorter than the acoustic wavelength can be neglected because they are destroyed by mixing more quickly. Modern LPRE combustion chambers operate at supercritical pressure, and some preheating of the propellants is common due to either the use of propellant as a coolant or partial preburning to drive a turbopump; thus, a single-phase fluid is considered with gaseous propellants injected into the combustion chamber. The mixing and chemical reaction are modelled. For the transverse mode, amplitude variations in the axial direction of the cylindrical configuration are considered to be sufficiently small to facilitate the reduction from a three-dimensional, unsteady problem to a two-dimensional, unsteady problem.

A. General Formulation of Theory

We use a wave dynamics model previously discussed in the literature. [2,11–15] Gravity and viscosity are neglected, and E is the time rate of energy per unit volume that is converted from a chemical form to a thermal form. A perfect gas and constant specific heats are assumed. Of course, at very high pressures, there should be corrections to the gas law, and at high temperatures, the specific heats should be variable. Nevertheless, the approximation is expected to allow a good description of the wave dynamics and the combustion dynamics without missing any primary physics. R is the specific gas constant for the mixture of gases in the chamber, T is the gas temperature, a is the speed of sound, c_p is the specific heat at constant pressure, c_v is the specific heat at constant volume, and $\gamma = c_p/c_v$. Although the temperature and therefore the sound speed vary significantly through the flame regions of mixing and reaction, we assume that wave propagation is controlled by the sound speed of the surrounding high-temperature product gases. Later, we specifically address small coaxial propellant jet streams of propellants, one jet for each injector, where the flames reside.

The previously described analysis yields [11]

$$\frac{\partial^2 p}{\partial t^2} - a^2 \frac{\partial^2 p}{\partial x_j \partial x_j} = \frac{\partial \rho}{\partial t}\frac{\partial a^2}{\partial t} + (\gamma - 1)\frac{\partial E}{\partial t} + a^2 \frac{\partial^2 (\rho u_j u_i)}{\partial x_i \partial x_j} \quad (1)$$

The left-hand side of the equation represents the wave operator in three dimensions with a mild nonlinearity appearing through the coefficient a^2. The first and third terms on the right-hand side are strongly nonlinear terms that are conservative but affect the wave shape. The second term on the right represents the influence of the energy conversion and can be a strong driver of the nonlinear oscillation.

B. Reduction to Two-Dimensional Wave Equation

Now, a two-dimensional model is developed, following Sirignano and Popov [11], by integrating Eq. (1) over the primary flow direction x_3. Focus is on the transverse-mode instability; so, the major oscillations are in the x_1 and x_2 directions. A cylindrical combustion chamber is considered with the injector at $x_3 = 0$ and the nozzle entrance at $x_3 = L$. Variations of the pressure, velocity, and other variables in the x_3 direction are smaller than variations in other directions.

The mass flux per unit area flowing from the injectors is considered to be a function of the local pressure at the exit of the injector, which is the injector face of the combustion chamber. So, $\rho u_3|_0 = g(p, x_1, x_2)$, where the function $g(p, x_1, x_2)$ can be determined by analysis of the flow in the orifice and upstream in the propellant feed system. For portions of the injector face where no orifice hole exists, $g = 0$.

A special nozzle configuration, which is achievable experimentally, is assumed: a multi-orifice flow exit with each orifice in a perforated plate in the exit plane being a small choked nozzle with a length much shorter than the oscillation wavelength and a residence time much shorter than the oscillation period. Under these conditions, the flow through the nozzle is quasi-steady. This nozzle boundary condition for nonlinear transverse waves was developed by Crocco and Sirignano [23,24]. The entrance Mach number of the nozzle is considered to be sufficiently low so that entrance stagnation values and static values are practically identical. Also, we neglect higher-order effects of the transverse velocity on the stagnation pressure of the nozzle inflow.

The pressure variation in the x_3 direction may be assumed to be minor for many transverse oscillations, especially if the mean-flow Mach number $M \ll 1$. The major variation of pressure will be in the transverse direction, as indicated by experimental findings [1] and theory [5,9]. For a pure transverse wave behavior, there is no acoustical oscillation in the x_3 direction; so, only advection can be expected to produce variations in that flow direction. These variations tend to be slow exponential variations according to the theory [5,9].

The nozzle boundary condition provides a first-time-derivative term that acts as a damping function for the oscillation. It represents the loss of some of the acoustic energy through the nozzle outflow. The term with the time derivative of the energy source E can be described as the forcing function for the oscillation. A combustion model will be developed to relate that quantity E back to pressure, temperature, and velocity. The other two nonlinear terms on the right-hand side of the equation are not dissipative or forcing functions, but they can have strong influence on the stability, amplitude, and wave shape for the oscillation.

It is assumed that the averaged pressure, temperature, density, and sound speed are related by polytropic relations. Additionally, isentropic relations are used to describe the thermodynamic relations during the oscillation. For transverse oscillations in a cylindrical chamber, shock waves do not form [1,2,5,9]. Also, the acoustic wavelengths are sufficiently long that viscous and diffusive effects are small, except for a combustion zone near an injector. These isentropic relations can be used to eliminate density, sound speed, and temperature from Eq. (1). The neglect of entropy variations in the determination of the pressure and velocity fields is not a very strong assumption. While entropy waves and other kinematic waves (e.g., flowing vortex structures) have been found significant in other combustors [6], they have not been found to be significant in LPRE operations.

It is useful to cast the two-dimensional construction of the wave dynamics equation in cylindrical polar coordinates because of the combustion chamber shape. The radial distance from the chamber centerline and azimuthal position will be represented by r and θ, respectively. The velocity components are u_r and u_θ,

$$\frac{\partial^2 p}{\partial t^2} + B_2 p^{\gamma-1/2\gamma}\frac{\partial p}{\partial t} - B_1 p^{\gamma-1/\gamma}\left[\frac{\partial^2 p}{\partial r^2} + \frac{1}{r}\frac{\partial p}{\partial r} + \frac{1}{r^2}\frac{\partial^2 p}{\partial \theta^2}\right]$$
$$= \frac{(\gamma-1)}{\gamma}\frac{1}{p}\left(\frac{\partial p}{\partial t}\right)^2 + (\gamma-1)\frac{\partial E}{\partial t}$$
$$+ \gamma p^{\gamma-1/\gamma}\left[\frac{\partial^2 (p^{1/\gamma}u_r^2)}{\partial r^2} + \frac{2}{r}\frac{\partial (p^{1/\gamma}u_r^2)}{\partial r}\right.$$
$$+ \frac{2}{r}\frac{\partial^2 (p^{1/\gamma}u_r u_\theta)}{\partial r \partial \theta} + \frac{2}{r^2}\frac{\partial (p^{1/\gamma}u_r u_\theta)}{\partial \theta} + \frac{1}{r^2}\frac{\partial^2 (p^{1/\gamma}u_\theta^2)}{\partial \theta^2}$$
$$\left. - \frac{1}{r}\frac{\partial (p^{1/\gamma}u_\theta^2)}{\partial r}\right] \tag{2}$$

where it is defined that

$$B_1 \equiv \frac{a_{ss}^2}{p_{ss}^{\gamma-1/\gamma}}; \qquad B_2 \equiv \frac{a_{ss}K}{L p_{ss}^{\gamma-1/2\gamma}}; \qquad K \equiv \frac{A_t}{A_e}\left(\frac{\gamma+1}{2}\right)^{\gamma-3/2(\gamma-1)} \tag{3}$$

Note that a one-dimensional isentropic flow analysis yields for the nozzle throat-to-entrance area ratio, after neglect of terms of $O(M^2)$,

$$\frac{A_t}{A_e} \approx M\left(\frac{\gamma+1}{2}\right)^{\gamma+1/2(\gamma-1)} \tag{4}$$

where M is the combustion chamber mean-flow Mach number with $0 < M \ll 1$. Thus, we approximate

$$K \approx M\left(\frac{\gamma+1}{2}\right); \qquad B_2 \approx M\frac{\gamma+1}{2}\frac{a_{ss}}{L p_{ss}^{\gamma-1/2\gamma}} \tag{5}$$

It is noteworthy that the nondimensional form of the quantity B_2 is small and positive if $M \ll 1$. Equation (2) neglects injector coupling and keeping the inflow mass flux constant under chamber oscillation. Popov et al. [13] have shown that injector coupling presents modest adjustments to the frequency and amplitude. However, a pulsed injector blockage could trigger an instability.

One may now cast the momentum equations in cylindrical coordinates to obtain

$$\frac{\partial u_r}{\partial t} + u_r\frac{\partial u_r}{\partial r} + u_\theta\frac{1}{r}\frac{\partial u_r}{\partial \theta} - \frac{u_\theta^2}{r} + \frac{C}{p^{1/\gamma}}\frac{\partial p}{\partial r} = 0 \tag{6}$$

and

$$\frac{\partial u_\theta}{\partial t} + u_r\frac{\partial u_\theta}{\partial r} + u_\theta\frac{1}{r}\frac{\partial u_\theta}{\partial \theta} + \frac{u_r u_\theta}{r} + \frac{C}{r p^{1/\gamma}}\frac{\partial p}{\partial \theta} = 0 \tag{7}$$

where $C \equiv p_{ss}^{1/\gamma}/\rho_{ss}$.

Consider a solid circular wall at radius $r = R$; that is, no acoustic lining is present. The normal velocity at the wall will be zero; so, the following boundary conditions apply to the system of Eqs. (2), (6), and (7):

$$u_r(t, R, \theta) = 0; \qquad \frac{\partial p}{\partial r}(t, R, \theta) = \frac{p^{1/\gamma}u_\theta^2}{CR} \tag{8}$$

The wave dynamics will be studied in Sec. III by using a postulated generalized relation between the heat release rate E and the pressure p with time delays allowed in the response of E to the pressure fluctuation. Use will be made later of a specific model of coaxial injection, turbulent mixing, and chemical reaction. This model will introduce physics with characteristic times that introduce time delays.

III. Two-Time-Variable Perturbation Method

The wave dynamics problem, now reduced to two transverse dimensions, presents the dependent variables as functions of the dimensional variables t, r, and θ without any dependence on the axial coordinate x. We nondimensionalize that reduced wave dynamics problem described by Eqs. (2), (6), and (7) and solve using the two-time-variable perturbation expansion method. Subscript ss will imply steady-state values, e.g., p_{ss}, a_{ss}, and E_{ss}. These values will be used to normalize the dependent variables, creating nondimensional forms: pressure will be normalized by the steady-state pressure p_{ss}, and velocity components will be normalized by the steady-state speed of sound a_{ss}, both having uniform values over the domain for the wave dynamics equation. The radial position will be normalized by the chamber radius R, and time is normalized by R/a_{ss}. From this point forward, for this section and the following section, the variables t, r, p, E, u_r, and u_θ should be interpreted as normalized, nondimensional quantities. A return in the later sections to dimensional variables will be made for the purposes of comparison with CFD results and introduction of the jet-flame model for the energy rate determination. Note that $a_{ss}^2 = \gamma p_{ss}/\rho_{ss}$, and the mean-flow Mach number $M = u_{ss}/a_{ss}$.

Two nondimensional time variables are introduced [25]: a fast-time variable $z = \omega t$ on which the oscillations occur and a slow-time variable $\tau = \sigma t$ on which amplitudes and phase slowly change. The angular frequency of oscillation is ω, and σ is a small positive quantity that goes to zero as the oscillation amplitude goes to zero. A dependent variables becomes a function of both variables: e.g., $p(z, \tau, r, \theta)$. Then, $\partial p/\partial t = \omega \partial p/\partial z + \sigma \partial p/\partial \tau$. Of course, the method only allows periodic behavior in the fast-time variable z and assumes the amplitude and phase will change more slowly. The method only applies for operating domains where the growth rate or decay rate (fractional change per unit time) is smaller by at least one order of magnitude than the oscillation frequency.

Equations (2), (6), and (7) are rewritten in nondimensional terms as

$$\omega^2\frac{\partial^2 p}{\partial z^2} - \left[\frac{\partial^2 p}{\partial r^2} + \frac{1}{r}\frac{\partial p}{\partial r} + \frac{1}{r^2}\frac{\partial^2 p}{\partial \theta^2}\right]$$
$$= -\omega\sigma\frac{\partial^2 p}{\partial z \partial \tau} - \sigma^2\frac{\partial^2 p}{\partial \tau^2} + (\gamma-1)\left[\omega\frac{\partial E}{\partial z} + \sigma\frac{\partial E}{\partial \tau}\right]$$
$$- B p^{\gamma-1/2\gamma}\left[\omega\frac{\partial p}{\partial z} + \sigma\frac{\partial p}{\partial \tau}\right] + N \tag{9}$$

where B is the nondimensional version of the dimensional B_2; thus,

$$B \approx M\frac{\gamma+1}{2}\frac{R}{L} \tag{10}$$

and the nonlinear acoustic terms are given as

$$N \equiv (p^{\gamma-1/\gamma} - 1)\left[\frac{\partial^2 p}{\partial r^2} + \frac{1}{r}\frac{\partial p}{\partial r} + \frac{1}{r^2}\frac{\partial^2 p}{\partial \theta^2}\right] + \frac{(\gamma-1)}{\gamma}\frac{1}{p}\left(\omega\frac{\partial p}{\partial z} + \sigma\frac{\partial p}{\partial \tau}\right)^2$$
$$+ \gamma p^{\gamma-1/\gamma}\left[\frac{\partial^2 (p^{1/\gamma}u_r^2)}{\partial r^2} + \frac{2}{r}\frac{\partial (p^{1/\gamma}u_r^2)}{\partial r} + \frac{2}{r}\frac{\partial^2 (p^{1/\gamma}u_r u_\theta)}{\partial r \partial \theta}\right.$$
$$\left. + \frac{2}{r^2}\frac{\partial (p^{1/\gamma}u_r u_\theta)}{\partial \theta} + \frac{1}{r^2}\frac{\partial^2 (p^{1/\gamma}u_\theta^2)}{\partial \theta^2} - \frac{1}{r}\frac{\partial (p^{1/\gamma}u_\theta^2)}{\partial r}\right] \tag{11}$$

The energy rate per volume E will be proportional to the mass flux of propellants for a fixed mixture ratio. For fixed mean values of chamber pressure and temperature, the mass flux will be proportional to the mean-flow Mach number M in the chamber. Thus, the quantity E can be expected also to go to zero as $M \to 0$. Furthermore, $\partial E/\partial t \to 0$ as the oscillation amplitude and/or M approaches zero.

With the placement of nonlinear terms on the right sides of the equations, the nondimensional momentum equations become

$$\omega\frac{\partial u_r}{\partial z} + \frac{1}{\gamma}\frac{\partial p}{\partial r} = -\sigma\frac{\partial u_r}{\partial \tau} - \left[u_r\frac{\partial u_r}{\partial r} + u_\theta\frac{1}{r}\frac{\partial u_r}{\partial \theta} - \frac{u_\theta^2}{r}\right]$$
$$+ \frac{1}{\gamma}\left[1 - \frac{1}{p^{1/\gamma}}\right]\frac{\partial p}{\partial r} \tag{12}$$

and

$$\omega\frac{\partial u_\theta}{\partial z}+\frac{1}{\gamma r}\frac{\partial p}{\partial\theta}=-\sigma\frac{\partial u_\theta}{\partial\tau}-\left[u_r\frac{\partial u_\theta}{\partial r}+u_\theta\frac{1}{r}\frac{\partial u_\theta}{\partial\theta}+\frac{u_r u_\theta}{r}\right]+\frac{1}{\gamma r}\left[1-\frac{1}{p^{1/\gamma}}\right]\frac{\partial p}{\partial\theta} \tag{13}$$

The nondimensional boundary conditions are given as

$$u_r(z,\tau,1,\theta)=0;\qquad \frac{\partial p}{\partial r}(z,\tau,1,\theta)=p^{1/\gamma}u_\theta^2 \tag{14}$$

An implicit constraint is the solution must remain finite without any singularity.

A perturbation expansion is assumed with ε as the perturbation parameter, which is a measure of oscillation amplitude. Specifically, we take

$$\begin{aligned}
p&=1+\varepsilon p_1(z,\tau,r,\theta)+\varepsilon^2 p_2(z,\tau,r,\theta)+\varepsilon^3 p_3(z,\tau,r,\theta)+O(\varepsilon^4)\\
u_r&=\varepsilon u_{r,1}(z,\tau,r,\theta)+\varepsilon^2 u_{r,2}(z,\tau,r,\theta)+\varepsilon^3 u_{r,3}(z,\tau,r,\theta)+O(\varepsilon^4)\\
u_\theta&=\varepsilon u_{\theta,1}(z,\tau,r,\theta)+\varepsilon^2 u_{\theta,2}(z,\tau,r,\theta)+\varepsilon^3 u_{\theta,3}(z,\tau,r,\theta)+O(\varepsilon^4)\\
\omega&=\omega_0+\varepsilon\omega_1+\varepsilon^2\omega_2+O(\varepsilon^3)\\
p^{\Gamma(\gamma)}&=1+\varepsilon\Gamma p_1+\varepsilon^2\left[\Gamma p_2+\frac{\Gamma(\Gamma-1)}{2}p_1^2\right]+O(\varepsilon^3)
\end{aligned} \tag{15}$$

The zeroeth-order solutions are the steady-state solutions; thus, the nondimensional $p_0=1$ and $u_{r,0}=u_{\theta,0}=0$. The last relation for p^Γ results from a Taylor series expansion in powers of $p-1$, followed by a substitution of the perturbation series for p.

The values of σ and ε will not be arbitrarily assigned. Rather, terms in the equations that result from the substitutions of the expansions of Eq. (15) into the wave and momentum equations governing the fluid motion will be ordered in a way to maximize the physics that is brought into the key descriptions of amplitude and phase of the oscillations. This principle will force definitions for the values of σ, ε, ω_1, ω_2, and other higher order constants. For example, to predict a behavior for the amplitude of the oscillation that allows determination of the limit cycle, any derived equation for the amplitude must balance linear terms with at least one nonlinear term. If we choose values for σ or ε that do not accomplish the balance, our physical representation is incomplete. It will be shown later in Secs. III.C and III.D that $\omega_1=0$ and $\sigma=M=\varepsilon^2$. For simplicity, those values will be taken now and proven later.

A. First-Order Equations

Now, we substitute Eq. (15) into Eqs. (9) and (11–13) and separate according to powers of ε. The resulting first-order equations [i.e., $O(\varepsilon)$] become

$$\omega_0^2\frac{\partial^2 p_1}{\partial z^2}-\left[\frac{\partial^2 p_1}{\partial r^2}+\frac{1}{r}\frac{\partial p_1}{\partial r}+\frac{1}{r^2}\frac{\partial^2 p_1}{\partial\theta^2}\right]=-(\gamma-1)\omega_0\frac{\partial E_{1,\mathrm{crit}}}{\partial z}-B\omega_0\frac{\partial p_1}{\partial z} \tag{16}$$

$$\omega_0\frac{\partial u_{r1}}{\partial z}+\frac{1}{\gamma}\frac{\partial p_1}{\partial r}=0 \tag{17}$$

$$\omega_0\frac{\partial u_{\theta1}}{\partial z}+\frac{1}{\gamma r}\frac{\partial p_1}{\partial\theta}=0 \tag{18}$$

$$u_{r1}(z,\tau,1,\theta)=0;\qquad \frac{\partial p_1}{\partial r}(z,\tau,1,\theta)=0 \tag{19}$$

Since the slow-time derivative is forced by its nature to be smaller and therefore of higher order than the fast-time derivative, the slow-time derivative does not appear to first order. The resonant modes for the chamber are described by the homogeneous form of Eq. (16). As currently stated, a homogeneous solution will appear on the right side as a forcing function. To maintain a finite solution, the two terms on the right side must cancel. That is, $E_{1,\mathrm{crit}}$ is the portion of the first-order perturbation of energy rate needed to balance the first-order nozzle damping. Thus, the right side of the equation becomes zero, yielding only the homogeneous solution. More details about E_1 and $E_{1,\mathrm{crit}}$ follow.

An infinite number of modes are possible, implying an infinite number of solutions for the first-order equations and, consequently, an infinite number of higher-order solutions. The most common and most destructive mode for a LPRE is the first tangential spinning mode, which we select here for examination. If we consider the right side of Eq. (16) to be zero, the first-order solutions are the classical results,

$$\begin{aligned}
p_1&=A(\tau)J_1(s_{11}r)\cos(z-\theta+\psi(\tau));\\
u_{r1}&=-\frac{A}{\gamma s_{11}}\frac{\mathrm{d}J_1}{\mathrm{d}r}\sin(z-\theta+\psi);\\
u_{\theta1}&=\frac{A}{\gamma s_{11}r}J_1\cos(z-\theta+\psi)\quad \omega_0=s_{11}=1.8413
\end{aligned} \tag{20}$$

where J_1, A, and ψ are the Bessel function of first kind and first order, slowly varying amplitude, and slowly varying phase angle, respectively.

The first five roots s_{1m} of the Bessel function $J_1(s_{1n}r)$ giving a zero slope of J_1 at $r=1$ are $s_{11}=1.8412$, $s_{12}=5.3313$, $s_{13}=8.5263$, $s_{14}=11.706$, and $s_{15}=14.864$. The lowest eigenvalue has been taken because it describes the first tangential mode. The other eigenvalues relate to modes with combined first tangential and first radial modes, combined first tangential and second radial modes, combined first tangential and third radial modes, and combined first tangential and fourth radial modes, respectively. Note that the Bessel function of the second kind has been discarded because it produces a singularity at $r=0$.

B. Asymptotic Order of Energy Release Rate

The energy release rate $E(z,\tau,r,\theta)$ must be expanded in a perturbation series. We consider it to be the sum of a steady-state portion plus a perturbation caused by the acoustic oscillation. Thus, $E=E_{\mathrm{ss}}(r,\theta)+E'(z,\tau,r,\theta)$, and $\partial E/\partial t=\partial E'/\partial t=\omega\partial E'/\partial z+\sigma\partial E'/\partial\tau$. Furthermore, we take $E'(z,\tau,r,\theta)=E'(\tau,r,z-\theta+\psi)$ for the travelling tangential wave. With the expectation that E' has components in phase and out of phase with pressure and that its amplitude is related to the pressure amplitude, the form

$$\begin{aligned}
E'(z,\tau,r,\theta)&=\Sigma_{n=0}^{\infty}\varepsilon^n A^n\{E_{c,n}(r)\cos[n(z-\theta+\psi)]+E_{s,n}(r)\sin[n(z-\theta+\psi)]\}\\
\frac{\partial E'}{\partial t}&=-\Sigma_{n=1}^{\infty}\varepsilon^n A^n s_{11}n\{E_{c,n}(r)\sin[n(z-\theta+\psi)]+E_{s,n}(r)\cos[n(z-\theta+\psi)]\}
\end{aligned} \tag{21}$$

is assumed, where the subscripts c and s designate coefficients of cosine and sine terms, respectively. Set

$$\begin{aligned}
E_{c,1}(r)&=\bar{E}_{c,1}J_1(s_{11}r)+\tilde{E}_{c,1}(r)\\
\bar{E}_{c,1}&\equiv\frac{\int_0^1 E_{c,1}(r)J_1(s_{11}r)r\,\mathrm{d}r}{\int_0^1 J_1^2(s_{11}r)r\,\mathrm{d}r}\\
\tilde{E}_{c,1}(r)&\equiv\Sigma_{m=2}^{\infty}\left[\frac{\int_0^1 E_{c,1}(r)J_1(s_{1\,m}r)r\,\mathrm{d}r}{\int_0^1 J_1^2(s_{1\,m}r)r\,\mathrm{d}r}\right]J_{1m}(r)
\end{aligned} \tag{22}$$

Now, we define $\bar{E}_{c,1,\text{excess}} = (\bar{E}_{c,1} - \bar{E}_{c,1,\text{crit}})/\varepsilon^2$, and separate the coefficient into two parts of different order in ε:

$$\bar{E}_{c,1} \equiv \bar{E}_{c,1,\text{crit}} + \varepsilon^2 \bar{E}_{c,1,\text{excess}} \tag{23}$$

The logic for the separation will become evident as we proceed through Secs. III.C and III.D. Realize that ε appears explicitly in Eq. (21) with the consequence that the right-side terms of Eq. (23) appear to first and third orders, respectively. We also consider $\bar{E}_{c,1}(r)$ to be of third order. Basically, these terms include components with cosinusoidal and sinusoidal variations at the fundamental frequency that can only find balancing terms at odd orders of ε. So, the value of ε must be determined so that the energy release mechanism appears to first and third orders. The nondimensional global energy release rate (i.e., integrated over the volume) is proportional to the nondimensional mass burning rate, which in turn is proportional to the propellant mass flow. Standard steady-state nozzle flow relations show that for $M \ll 1$ with a constant chamber cross-sectional area, pressure, and temperature both the mass flux and chamber Mach number decrease in proportion as throat area increases. Examination from a different perspective shows the same result: the mass burning rate is nondimensionalized using steady-state density and sound speed values in the combustion chamber, and, consequently, the nondimensional energy release rate is directly proportional to the chamber mean-flow Mach number. This will lead to a matching of ε^2 with M. Essentially, we are setting $\varepsilon = \sqrt{M}$. Physically, this is realistic because, as shall be shown in Sec. III.D, the lowest frequency terms appear only to odd orders in ε. Thereby, the necessary balance of certain terms is that the amplitude must adjust to the Mach-number value. The nondimensional amplitudes of the first-tangential-mode pressure oscillations will be defined as $\varepsilon A(\tau)J_1(s_{11}r) = \sqrt{M}A(\tau)J_1(s_{11}r)$. The case with $M \ll 1$ is of general practical interest.

$E_{s,1}(r)$ is also expanded in an eigenfunction series and considered to be of $O(\varepsilon^2)$

$$\begin{aligned} E_{s,1}(r) &= \varepsilon^2 \bar{E}_{s,1} J_1(s_{11}r) + \varepsilon^2 \tilde{E}_{s,1}(r) \\ \bar{E}_{s,1} &\equiv \frac{\int_0^1 E_{s,1}(r) J_1(s_{11}r) r\,\mathrm{d}r}{\varepsilon^2 \int_0^1 J_1^2(s_{11}r) r\,\mathrm{d}r} \\ \tilde{E}_{s,1}(r) &\equiv \Sigma_{m=2}^{\infty} \left[\frac{\int_0^1 E_{s,1}(r) J_1(s_{1m}r) r\,\mathrm{d}r}{\varepsilon^2 \int_0^1 J_1^2(s_{1m}r) r\,\mathrm{d}r} \right] J_{1m}(r) \end{aligned} \tag{24}$$

The result from setting the right side of Eq. (16) to be zero with substitution from Eqs. (20) and (21) is

$$\begin{aligned} &(\gamma - 1)\omega_0 A \bar{E}_{c,1,\text{crit}} J_1(s_{11}r) \sin(z - \theta + \psi) = -B\omega_0 \frac{\partial p_1}{\partial z} \\ &\quad = AB\omega_0 J_1(s_{11}r) \sin(z - \theta + \psi) \end{aligned} \tag{25}$$

Thus, the definition for the critical value is obtained whereby $\bar{E}_{c,1,\text{crit}} = B/(\gamma - 1)$ and $\varepsilon^2 \bar{E}_{c,1,\text{excess}} \equiv \bar{E}_{c,1} - B/(\gamma - 1)$. Essentially, the critical value balances the first-order value for the nozzle damping. The difference of $E_{c,1}$ from its critical value, namely, $E_{c,1,\text{excess}}$ will appear to higher order and will affect the limit-cycle amplitude. The higher-order terms for nozzle damping will balance with $E_{c,1,\text{excess}}$ at third order.

The physical interpretation from linear theory is that if $\bar{E}_{c,1} > \bar{E}_{c,1,\text{crit}}$ any small disturbance causes a growing exponential oscillation; if $\bar{E}_{c,1} < \bar{E}_{c,1,\text{crit}}$, any small disturbance causes a decaying exponential oscillation; and if $\bar{E}_{c,1} = \bar{E}_{c,1,\text{crit}}$, a neutral oscillation results. However, exponential solutions cannot predict the nonlinear limit cycles. We must bring the nonlinear physics into the balance to predict limit cycles and transients to stable limit cycles or away from unstable limit cycles. $E_{c,1,\text{excess}}$ will be balanced at higher order only with the nonlinear terms from the nozzle damping. Since the only driving and damping mechanisms in the model appear from combustion and nozzle outflow, respectively, there would only be potential flow in their absence. An interesting result is that a first-order (i.e., linear) theory for $E_{c,1,\text{excess}}$ is sufficient for a third-order analysis of the oscillation by a first-order (i.e., linear) theory for the oscillatory combustion process.

In the choice of the asymptotic sequence for the expansion here, we treat B as a parameter to be specified. Only after the perturbation expansion is applied and the separated equations for each order are established do we consider the dependence of B on M. Essentially, we have expanded the parameter space and treated M in some locations in the analysis as a different parameter from M appearing in other locations. This can raise mathematical questions on the behavior as ε goes to the zero limit. However, if the asymptotic series gives a decent engineering approximation to the behavior, no problem is expected.

C. Second-Order Equations

With the substitution from Eq. (15) into Eqs. (9) and (11–13) and separation according to powers of ε, the wave equation for the second-order pressure perturbation is yielded as follows:

$$\begin{aligned} &\omega_0^2 \frac{\partial^2 p_2}{\partial z^2} - \left[\frac{\partial^2 p_2}{\partial r^2} + \frac{1}{r}\frac{\partial p_2}{\partial r} + \frac{1}{r^2}\frac{\partial^2 p_2}{\partial \theta^2} \right] \\ &\quad = N_2 + Bs_{11} \left\{ A^2 \frac{\gamma - 1}{4\gamma} J_1^2(s_{11}r) \sin[2(z - \theta + \psi)] - \frac{\partial p_2}{\partial z} \right\} \end{aligned} \tag{26}$$

where

$$\begin{aligned} N_2 \equiv{}& \frac{\gamma - 1}{\gamma} p_1 \left[\frac{\partial^2 p_1}{\partial r^2} + \frac{1}{r}\frac{\partial p_1}{\partial r} + \frac{1}{r^2}\frac{\partial^2 p_1}{\partial \theta^2} \right] + \frac{(\gamma - 1)}{\gamma} \left(s_{11} \frac{\partial p_1}{\partial z} \right)^2 \\ &+ \gamma \left[\frac{\partial^2 (u_{r1}^2)}{\partial r^2} + \frac{2}{r}\frac{\partial (u_{r1}^2)}{\partial r} + \frac{2}{r}\frac{\partial^2 (u_{r1}u_{\theta 1})}{\partial r \partial \theta} + \frac{2}{r^2}\frac{\partial (u_{r1}u_{\theta 1})}{\partial \theta} \right. \\ &\left. + \frac{1}{r^2}\frac{\partial^2 (u_{\theta 1}^2)}{\partial \theta^2} - \frac{1}{r}\frac{\partial (u_{\theta 1}^2)}{\partial r} \right] \end{aligned} \tag{27}$$

Note that the energy release rate does not appear to this order; nor do the slow-time derivative terms appear. If these terms were included to this order, their exclusion by balancing would only give a linear equation for the temporal behaviors of $A(\tau)$ and $\psi(\tau)$. Triggering thresholds could not be predicted at this order. That is, if $\bar{E}_{c1,\text{excess}}$ were allowed a component of $O(\varepsilon)$ and appeared in this second-order Eq. (26), there would be a term in its forcing function proportional to $\sin(z - \theta + \psi)$, and this would be the only sine term of that frequency, other than a slow-time derivative term. (The nozzle damping represented through the first-time derivative of pressure manifests at other frequencies in this second-order balance.) This situation could not be allowed since it causes resonance; however, forcing the terms to balance only produces a linear ordinary differential equation for A with an exponential solution. Thus, the excess energy term and the slow-time derivative must be higher order in ε as portrayed in Eq. (23). These terms will be allowed to appear to third order, at which they can be balanced with a nonlinear term, giving a more meaningful and broader description of the behavior. By deferring the appearance of the excess energy release rate and the slow-time derivatives to third order, we are following the asymptotic balancing principle of combining as many terms (and accordingly as much physics) as possible.

The second-order momentum equations are

$$s_{11}\frac{\partial u_{r2}}{\partial z} + \frac{1}{\gamma}\frac{\partial p_2}{\partial r} = -\left[u_{r1}\frac{\partial u_{r1}}{\partial r} + u_{\theta 1}\frac{1}{r}\frac{\partial u_{r1}}{\partial \theta} - \frac{u_{\theta 1}^2}{r} \right] + \frac{1}{\gamma^2} p_1 \frac{\partial p_1}{\partial r} \tag{28}$$

and

$$s_{11}\frac{\partial u_{\theta 2}}{\partial z}+\frac{1}{\gamma r}\frac{\partial p_2}{\partial \theta}=-\left[u_{r1}\frac{\partial u_{\theta 1}}{\partial r}+u_{\theta 1}\frac{1}{r}\frac{\partial u_{\theta 1}}{\partial \theta}+\frac{u_{r1}u_{\theta}}{r}\right]+\frac{1}{\gamma^2 r}p_1\frac{\partial p_1}{\partial \theta} \tag{29}$$

$$u_{r2}(z,\tau,1,\theta)=0; \qquad \frac{\partial p_2}{\partial r}(z,\tau,1,\theta)=\gamma u_{\theta 1}^2(z,\tau,r,\theta) \tag{30}$$

Now, substitution of the first-order solution from Eq. (20) into Eq. (27) is possible. Standard trigonometric relations are used for simplifications; e.g., $(\cos x)^2=(1/2)[1+\cos(2x)]$. To remove derivatives from the result, repeated use of the following identity is made

$$\frac{\mathrm{d}J_n(s_{11}r)}{\mathrm{d}r}=\frac{n}{r}J_n(s_{11}r)-s_{11}J_{n+1}(s_{11}r) \tag{31}$$

and the evaluation of N_2 yields

$$\begin{aligned}N_2&=A^2q_0(r)+A^2q_2(r)\cos[2(z-\theta+\psi)]\\&=-A^2\frac{Q_0(r)}{r^2}-A^2\frac{Q_2(r)}{r^2}\cos[2(z-\theta+\psi)]\end{aligned} \tag{32}$$

where $Q_n(r)=-r^2q_n(r)$. The $q_n(r)$ functions are defined in Appendix A.

If ω_1 were kept in the expansion, Eq. (26) would have a term with the product of $\cos(z-\theta+\psi)$ and ω_1 on the right side. Furthermore, it would be the only cosine component with that frequency in the forcing function of that equation. That situation would force a resonant solution for p_2 that cannot be allowed. Thus, $\omega_1=0$ is required.

We have the second-order pressure particular solution to Eq. (26) created by the N_2 forcing function in the form

$$p_2^*=A^2F_0(r)+A^2F_2(r)\cos[2(z-\theta+\psi)] \tag{33}$$

The asterisk is used to identify an intermediate (i.e., incomplete) solution for p_2. Substitution of Eq. (33) into Eq. (26) and the separation according to linearly independent functions of z yield the ordinary differential equations

$$r^2\frac{\mathrm{d}^2F_0}{\mathrm{d}r^2}+r\frac{\mathrm{d}F_0}{\mathrm{d}r}=Q_0(r) \tag{34}$$

and

$$r^2\frac{\mathrm{d}^2F_2}{\mathrm{d}r^2}+r\frac{\mathrm{d}F_2}{\mathrm{d}r}+4(s_{11}^2r^2-1)F_2=Q_2(r) \tag{35}$$

Equation (34) can be solved by two successive integrations of first-order equations using integrating factors. However, another approach related to the solution of the second-order, radial momentum equation will be used later in this section.

Equation (35) can be solved by variation of parameters, reducing the solution to the sum of two quadratures. The homogeneous solutions to that differential equation are the Bessel function of the first kind $J_2(2s_{11}r)$ and of the second kind $Y_2(2s_{11}r)$. With $\zeta\equiv 2s_{11}r$, the Wronskian is given as $W=2/(\pi\zeta)=1/(\pi s_{11}r)$ [26]. Thus, the particular solution is given by

$$\begin{aligned}F_2(r)&=Y_2(2s_{11}r)\int_0^{2s_{11}r}\frac{J_2(\zeta)Q_2[\zeta/(2s_{11})]}{W(\zeta)[\zeta/(2s_{11})]^2}\,\mathrm{d}\zeta\\&\quad-J_2(2s_{11}r)\int_0^{2s_{11}r}\frac{Y_2(\zeta)Q_2[\zeta/(2s_{11})]}{W(\zeta)[\zeta/(2s_{11})]^2}\,\mathrm{d}\zeta\\&=2\pi s_{11}^2\left[Y_2(2s_{11}r)\int_0^r\frac{J_2(2s_{11}r')Q_2(r')}{r'}\,\mathrm{d}r'\right.\\&\quad\left.-J_2(2s_{11}r)\int_0^r\frac{Y_2(2s_{11}r')Q_2(r')}{r'}\,\mathrm{d}r'\right]\end{aligned} \tag{36}$$

The first term has a singularity at $r=0$ introduced through Y_2. However, an expansion of $Q_2(r)$ for small r shows that it is $O(r^2)$ in the limit as $r\to 0$. Thus, the multiplying integral will behave as r^4 for a small radius, thereby removing the singularity through the product. In the second term, the integrand is singular, and the integral will be singular. Again, the product formed with J_2 removes the singular behavior. The lower limits on the integrals are set to zero to avoid discontinuities at $r=0$. That is, a finite value of $F_2(0)$ multiplied by the cosine function would result in discontinuous behavior for $p_2(z,0,\theta)$.

The remaining particular solution to Eq. (26) will be obtained using $p_2\approx p_2^*$ to substitute on the right side of that equation, which is justified because $B=O(M)$, where the mean-flow Mach number M is small compared to unity. The forcing function on the right-hand side of Eq. (26) now becomes

$$\begin{aligned}&A^2q_0(r)+A^2q_2(r)\cos[2(z-\theta+\psi)]+A^2q_{2s}\sin[2(z-\theta+\psi)]\\&\quad=-\frac{A^2}{r^2}\{Q_0(r)+Q_2(r)\cos[2(z-\theta+\psi)]\\&\qquad+Q_{2s}\sin[2(z-\theta+\psi)]\}\end{aligned} \tag{37}$$

where

$$Q_{2s}\equiv -Bs_{11}r^2\left[2F_2(r)+\frac{\gamma-1}{4\gamma}J_1^2(s_{11}r)\right] \tag{38}$$

Consideration of the additional term in the forcing function for Eq. (26) implies that an additional particular solution of the form $F_{2s}(r)\sin[2(z-\theta+\psi)]$ must be added to the solution. The differential equation for F_{2s} is

$$\begin{aligned}r^2\frac{\mathrm{d}^2F_{2s}}{\mathrm{d}r^2}+r\frac{\mathrm{d}F_{2s}}{\mathrm{d}r}+4(s_{11}^2r^2-1)F_{2s}&=Q_{2s}(r)\\&=-Bs_{11}r^2\left[2F_2(r)+\frac{\gamma-1}{4\gamma}J_1^2(s_{11}r)\right]\end{aligned} \tag{39}$$

Now, with substitution from Eq. (36), we determine the solution F_{2s} for Eq. (39) using the variation-of-parameters method:

$$\begin{aligned}F_{2s}(r)&=2\pi s_{11}^2\left[Y_2(2s_{11}r)\int_0^r\frac{J_2(2s_{11}r')Q_{2s}(r')}{r'}\,\mathrm{d}r'\right.\\&\quad\left.-J_2(2s_{11}r)\int_0^r\frac{Y_2(2s_{11}r')Q_{2s}(r')}{r'}\,\mathrm{d}r'\right]\end{aligned} \tag{40}$$

For similar reasons to those for the F_2 case, we have no singularity in this solution for F_{2s}.

Adding $F_{2s}\sin[2(z-\theta+\psi)]$ to p_2^* from Eq. (33), we now have

$$\begin{aligned}p_2&=A^2F_0(r)+A^2F_2(r)\cos[2(z-\theta+\psi)]\\&\quad+A^2F_{2s}(r)\sin[2(z-\theta+\psi)]\end{aligned} \tag{41}$$

In the following analysis, the argument for any J_n Bessel function will be implied to be $s_{11}r$ unless explicitly defined as otherwise. The solution of Eq. (28) for u_{r2} can be obtained by first substituting solutions for u_{r1}, $u_{\theta 1}$, and p_2 to obtain

$$\frac{\partial u_{r2}}{\partial z} = \frac{A^2}{\gamma^2 s_{11}^2}\left[\frac{J_1 J_2}{r^2} - \frac{s_{11}J_2^2}{2r} - \gamma s_{11}\frac{\mathrm{d}F_2}{\mathrm{d}r}\right]\cos[2(z-\theta+\psi)]$$
$$- \frac{A^2}{\gamma s_{11}}\frac{\mathrm{d}F_{2s}}{\mathrm{d}r}\sin[2(z-\theta+\psi)]$$
$$+ \frac{A^2}{\gamma s_{11}}\left\{-\frac{\mathrm{d}F_0}{\mathrm{d}r} + \frac{1}{\gamma}\left(1 - \frac{1}{s_{11}^2 r^2}\right)J_1\frac{\mathrm{d}J_1}{\mathrm{d}r}\right.$$
$$\left. + \frac{1}{2\gamma r s_{11}^2}\left[\left(\frac{\mathrm{d}J_1}{\mathrm{d}r}\right)^2 + \left(\frac{J_1}{r}\right)^2\right]\right\} \tag{42}$$

Now, to prevent u_{r2} from growing toward infinity with transformed time z, it is necessary that the last line of the previous equation becomes identically zero. Thus, F_0 must satisfy the first-order differential equation

$$\frac{\mathrm{d}F_0}{\mathrm{d}r} = \frac{1}{\gamma}\left(1 - \frac{1}{s_{11}^2 r^2}\right)J_1\frac{\mathrm{d}J_1}{\mathrm{d}r} + \frac{1}{2\gamma r s_{11}^2}\left[\left(\frac{\mathrm{d}J_1}{\mathrm{d}r}\right)^2 + \left(\frac{J_1}{r}\right)^2\right] \tag{43}$$

It can be shown by differentiation and substitution into Eq. (34) that if F_0 satisfies Eq. (43) it also satisfies Eq. (34). With expected uniqueness for the solution to the differential equation, the solution satisfies both the differential equation (34) and the condition (43). So, there is no conflict between Eqs. (34) and (43), and the solution for u_{r2} becomes

$$u_{r2} = A^2 G_2(r)\sin[2(z-\theta+\psi)] + A^2 G_{2s}(r)\cos[2(z-\theta+\psi)]$$
$$G_2(r) \equiv \frac{1}{2\gamma^2 s_{11}^2}\left[\frac{J_1 J_2}{r^2} - \frac{s_{11}J_2^2}{2r} - \gamma s_{11}\frac{\mathrm{d}F_2}{\mathrm{d}r}\right];$$
$$G_{2s}(r) \equiv \frac{1}{2\gamma s_{11}}\frac{\mathrm{d}F_{2s}}{\mathrm{d}r} \tag{44}$$

The solution of Eq. (29) for $u_{\theta 2}$ can readily be obtained by substituting solutions for u_{r1}, $u_{\theta 1}$, and p_2 and integrating over z. The constant of integration (actually allowed to be a function of r) is set to zero by the condition of zero vorticity (zero circulation) to this order of the perturbation series. The result is

$$u_{\theta 2} = A^2 H_2(r)\cos[2(z-\theta+\psi)] + A^2 H_{2s}(r)\sin[2(z-\theta+\psi)]$$
$$H_2(r) \equiv \frac{1}{\gamma s_{11} r}\left[F_2 + \frac{J_1^2 - J_2^2}{4\gamma} + \frac{J_1 J_2}{2\gamma s_{11} r}\right];$$
$$H_{2s}(r) \equiv \frac{1}{\gamma s_{11} r}F_{2s} \tag{45}$$

Equation (43) can be integrated to obtain F_0 with the result

$$F_0 = K + \frac{J_1^2}{2\gamma} + \frac{1}{2\gamma}\int_0^r\left[\frac{J_2^2}{r'} - \frac{2J_1 J_2}{s_{11}(r')^2}\right]\mathrm{d}r' \tag{46}$$

The constant of integration K can be determined by the constraint that the instantaneous value of the integral of the density over the chamber volume remains constant during pressure oscillation, yielding the same mass as given in steady-state operation. In particular, density is related to pressure through an isentropic approximation, and using Eq. (15) with $\Gamma = \gamma$, an expansion for density through second order is obtained and integrated over the chamber volume. All terms with sine and cosine functions integrate to zero. Thus, we have

$$\int_0^1 rF_0\,\mathrm{d}r = \frac{\gamma-1}{4\gamma}\int_0^1 rJ_1^2\,\mathrm{d}r \tag{47}$$

Consequently,

$$K = \frac{\gamma-3}{2\gamma}\int_0^1 rJ_1^2\,\mathrm{d}r + \frac{1}{\gamma}\int_0^1\left\{\int_0^r\left[\frac{2J_1J_2}{s_{11}(r')^2} - \frac{J_2^2}{r'}\right]\mathrm{d}r'\right\}r\,\mathrm{d}r \tag{48}$$

D. Third-Order Equations

Following the established pattern, the wave equation for the third-order pressure perturbation is obtained following the substitution from Eq. (15) into Eqs. (9) and (11–13) and separation according to powers of ε. The condition $\sigma(\varepsilon) = \varepsilon^2$ has been taken, thereby introducing the slow time derivatives in the third-order equations. At this third order, there will be other sine and cosine terms of the basic frequency appearing in the forcing function to balance the terms proportional to σ. These proportional terms involve derivatives of amplitude A and phase ψ with respect to the slow time. Thus, $\sigma(\varepsilon) = \varepsilon^2$ is chosen, following the established principle in asymptotic analysis to choose orders so as to include and balance the most terms (and thereby the most physics). Similarly, the frequency correction ω_2 is included here in the balance.

The third-order equations follow:

$$\omega_0^2\frac{\partial^2 p_3}{\partial z^2} - \left[\frac{\partial^2 p_3}{\partial r^2} + \frac{1}{r}\frac{\partial p_3}{\partial r} + \frac{1}{r^2}\frac{\partial^2 p_3}{\partial\theta^2}\right]$$
$$= -2\omega_0\omega_2\frac{\partial^2 p_1}{\partial z^2} - \omega_0\frac{\partial^2 p_1}{\partial z\partial\tau} + (\gamma-1)\omega_0\frac{\partial E_3}{\partial z}$$
$$- B\omega_0\left[\frac{\partial p_3}{\partial z} + \frac{\gamma-1}{2\gamma}\left(p_2\frac{\partial p_1}{\partial z} + p_1\frac{\partial p_2}{\partial z}\right) + \frac{\gamma^2-1}{8\gamma^2}p_1^2\frac{\partial p_1}{\partial z}\right]$$
$$+ N_3 \tag{49}$$

$$N_3 \equiv \frac{\gamma-1}{\gamma}p_1\left[\frac{\partial^2 p_2}{\partial r^2} + \frac{1}{r}\frac{\partial p_2}{\partial r} + \frac{1}{r^2}\frac{\partial^2 p_2}{\partial\theta^2}\right]$$
$$+ \left(\frac{\gamma-1}{\gamma}p_2 - \frac{\gamma-1}{2\gamma^2}p_1^2\right)\left[\frac{\partial^2 p_1}{\partial r^2} + \frac{1}{r}\frac{\partial p_1}{\partial r} + \frac{1}{r^2}\frac{\partial^2 p_1}{\partial\theta^2}\right]$$
$$+ \frac{2(\gamma-1)}{\gamma}\left(\omega_0^2\frac{\partial p_1}{\partial z}\frac{\partial p_2}{\partial z}\right) - \frac{(\gamma-1)}{\gamma}p_1\left(\omega_0\frac{\partial p_1}{\partial z}\right)^2$$
$$+ 2\gamma\left[\frac{\partial^2(u_{r1}u_{r2})}{\partial r^2} + \frac{2}{r}\frac{\partial(u_{r1}u_{r2})}{\partial r} + \frac{1}{r}\frac{\partial^2(u_{r2}u_{\theta1} + u_{r1}u_{\theta2})}{\partial r\partial\theta}\right.$$
$$\left. + \frac{1}{r^2}\frac{\partial(u_{r2}u_{\theta1} + u_{r1}u_{\theta2})}{\partial\theta} + \frac{1}{r^2}\frac{\partial^2(u_{\theta1}u_{\theta2})}{\partial\theta^2} - \frac{1}{r}\frac{\partial(u_{\theta1}u_{\theta2})}{\partial r}\right]$$
$$+ (\gamma-1)p_1\left[\frac{\partial^2(u_{r1}^2)}{\partial r^2} + \frac{2}{r}\frac{\partial(u_{r1}^2)}{\partial r} + \frac{2}{r}\frac{\partial^2(u_{r1}u_{\theta1})}{\partial r\partial\theta}\right.$$
$$\left. + \frac{2}{r^2}\frac{\partial(u_{r1}u_{\theta1})}{\partial\theta} + \frac{1}{r^2}\frac{\partial^2(u_{\theta1}^2)}{\partial\theta^2} - \frac{1}{r}\frac{\partial(u_{\theta1}^2)}{\partial r}\right]$$
$$+ \left[\frac{\partial^2(p_1u_{r1}^2)}{\partial r^2} + \frac{2}{r}\frac{\partial(p_1u_{r1}^2)}{\partial r} + \frac{2}{r}\frac{\partial^2(p_1u_{r1}u_{\theta1})}{\partial r\partial\theta}\right.$$
$$\left. + \frac{2}{r^2}\frac{\partial(p_1u_{r1}u_{\theta1})}{\partial\theta} + \frac{1}{r^2}\frac{\partial^2(p_1u_{\theta1}^2)}{\partial\theta^2} - \frac{1}{r}\frac{\partial(p_1u_{\theta1}^2)}{\partial r}\right] \tag{50}$$

$$\frac{\partial p_3}{\partial r}(z,\tau,1,\theta) = 2u_{\theta1}u_{\theta2} + \frac{1}{\gamma}p_1u_{\theta1}^2 \tag{51}$$

The first- and second-order solutions may be substituted into N_3 to yield

$$N_3(r, z-\theta+\psi) = A^3 q_1(r)\cos(z-\theta+\psi) + A^3 q_3(r)\cos[3(z-\theta+\psi)] + A^3 q_{1s}(r)\sin(z-\theta+\psi) + A^3 q_{3s}(r)\sin[3(z-\theta+\psi)] \quad (52)$$

where the $q_n(r)$ functions are defined in Appendix A.

The derivatives of F_2 and F_{2s} can be obtained by differentiation of the relations given in Eqs. (36) and (40). Then, the second derivatives can be obtained in terms of F_2 and F_{2s} from the differential equations, (35) and (39). The functions G_2, G_{2s}, H_2, and H_{2s} can be differentiated directly from their forms in Eqs. (44) and (45). Equation (31) is repeatedly used to replace derivatives of Bessel functions. See the results for those substitutions and analytical steps in Appendix A.

Using the functions q_1, q_{1s}, q_3, and q_{3s} defined in Appendix A, the forcing function on the right side of Eq. (49) is given by

$$\begin{aligned}
&-s_{11}A(\gamma-1)\bar{E}_{c,1,\text{excess}}J_1(s_{11}r)\sin(z-\theta+\psi)\\
&+s_{11}A(\gamma-1)\bar{E}_{s,1}J_1(s_{11}r)\cos(z-\theta+\psi)\\
&+2s_{11}\omega_2 A J_1(s_{11}r)\cos(z-\theta+\psi)\\
&+s_{11}\frac{\mathrm{d}A}{\mathrm{d}\tau}J_1(s_{11}r)\sin(z-\theta+\psi)\\
&+\frac{\mathrm{d}\psi}{\mathrm{d}\tau}s_{11}AJ_1(s_{11}r)\cos(z-\theta+\psi)\\
&-A^3Bs_{11}\left\{\frac{\partial p_3}{\partial z}+\frac{\gamma-1}{4\gamma}[2F_0J_1+F_2J_1]\sin[z-\theta+\psi]\right.\\
&\left.+3\frac{\gamma-1}{4\gamma}F_2J_1\sin[3(z-\theta+\psi)]\right\}\\
&-A^3Bs_{11}\left\{\frac{\gamma^2-1}{32\gamma^2}J_1^3\sin(z-\theta+\psi)+\frac{\gamma^2-1}{32\gamma^2}J_1^3\sin[3(z-\theta+\psi)]\right\}\\
&+A^3q_1(r)\cos(z-\theta+\psi)+A^3q_3(r)\cos[3(z-\theta+\psi)]\\
&+A^3q_{1s}(r)\sin(z-\theta+\psi)+A^3q_{3s}(r)\sin[3(z-\theta+\psi)] \quad (53)
\end{aligned}$$

The $J_1\sin(z-\theta+\psi)$ and $J_1\cos(z-\theta+\psi)$ eigenfunction terms cannot appear in the forcing function because they are homogeneous solutions for the partial differential equation (49). Their appearance would cause nonlinear resonance and not allow periodic solutions in the fast variable. So, the coefficients of those two eigenfunctions must be collected and balanced to give zero value. Thus, two constraints are established,

$$\begin{aligned}
\frac{\mathrm{d}A}{\mathrm{d}\tau} &= A(\gamma-1)\bar{E}_{c,1,\text{excess}}\\
&+A^3B\left[\frac{\gamma-1}{4\gamma}\frac{\int_0^1(2F_0J_1^2+F_2J_1^2)r\,\mathrm{d}r}{\int_0^1J_1^2r\,\mathrm{d}r}+\frac{\gamma^2-1}{32\gamma^2}\frac{\int_0^1J_1^4r\,\mathrm{d}r}{\int_0^1J_1^2r\,\mathrm{d}r}\right]\\
&-A^3\frac{\int_0^1q_{1s}(r)J_1(s_{11}r)r\,\mathrm{d}r}{s_{11}\int_0^1J_1^2(s_{11}r)r\,\mathrm{d}r} \quad (54)
\end{aligned}$$

$$\frac{\mathrm{d}\psi}{\mathrm{d}\tau} = -2\omega_2-(\gamma-1)\bar{E}_{s,1}-A^2\frac{\int_0^1q_1(r)J_1(s_{11}r)r\,\mathrm{d}r}{s_{11}\int_0^1J_1^2(s_{11}r)r\,\mathrm{d}r} \quad (55)$$

and the modified third-order wave equation becomes

$$\begin{aligned}
&\omega_0^2\frac{\partial^2p_3}{\partial z^2}-\left[\frac{\partial^2p_3}{\partial r^2}+\frac{1}{r}\frac{\partial p_3}{\partial r}+\frac{1}{r^2}\frac{\partial^2p_3}{\partial\theta^2}\right]\\
&=-A^3Bs_{11}\left\{\frac{\partial p_3}{\partial z}+3\frac{\gamma-1}{4\gamma}F_2J_1\sin[3(z-\theta+\psi)]\right\}\\
&-A^3Bs_{11}\frac{\gamma^2-1}{32\gamma^2}J_1^3\sin[3(z-\theta+\psi)]\\
&+A^3Bs_{11}\frac{\gamma-1}{4\gamma}\sum_{m\neq1}\frac{\int_0^1[2F_0J_1(s_{11}r)+F_2J_1(s_{11}r)]J_1(s_{1m}r)r\,\mathrm{d}r}{\int_0^1J_1^2(s_{1m}r)r\,\mathrm{d}r}\\
&\times J_1(s_{1m}r)\sin(z-\theta+\psi)\\
&-A^3Bs_{11}\frac{\gamma^2-1}{32\gamma^2}\sum_{m\neq1}\frac{\int_0^1J_1^3(s_{11}r)J_1(s_{1m}r)r\,\mathrm{d}r}{\int_0^1J_1^2(s_{1m}r)r\,\mathrm{d}r}J_1(s_{1m}r)\sin(z-\theta+\psi)\\
&+A^3\sum_{m\neq1}\frac{\int_0^1q_1(r)J_1(s_{1m}r)r\,\mathrm{d}r}{s_{11}\int_0^1J_1^2(s_{1m}r)r\,\mathrm{d}r}J_1(s_{1m}r)\cos(z-\theta+\psi)\\
&+A^3q_3(r)\cos[3(z-\theta+\psi)]\\
&+A^3\sum_{m\neq1}\frac{\int_0^1q_{1s}(r)J_1(s_{1m}r)r\,\mathrm{d}r}{s_{11}\int_0^1J_1^2(s_{1m}r)r\,\mathrm{d}r}J_1(s_{1m}r)\sin(z-\theta+\psi)\\
&+A^3q_{3s}(r)\sin[3(z-\theta+\psi)] \quad (56)
\end{aligned}$$

It is not necessary to obtain the solutions for p_3, $u_{\theta3}$, and u_{r3} in order to achieve the first approximation at growth and decay rates of the oscillation. The limit-cycle amplitude A^* and frequency perturbation ω_2 are given by setting the derivatives in Eqs. (54) and (55) equal to zero:

$$A^{*2} = (\gamma-1)\bar{E}_{c,1,\text{excess}}\left\{\frac{\int_0^1q_{1s}(r)J_1(s_{11}r)r\,\mathrm{d}r}{s_{11}\int_0^1J_1^2(s_{11}r)r\,\mathrm{d}r} -B\left[\frac{\gamma-1}{4\gamma}\frac{\int_0^1(2F_0J_1+F_2J_1)r\,\mathrm{d}r}{\int_0^1J_1^2r\,\mathrm{d}r}+\frac{\gamma^2-1}{32\gamma^2}\frac{\int_0^1J_1^4r\,\mathrm{d}r}{\int_0^1J_1^2r\,\mathrm{d}r}\right]\right\}-1 \quad (57)$$

$$\omega_2 = -(\gamma-1)\bar{E}_{s,1}-A^{*2}\frac{\int_0^1q_1(r)J_1(s_{11}r)r\,\mathrm{d}r}{2s_{11}\int_0^1J_1^2(s_{11}r)r\,\mathrm{d}r} \quad (58)$$

Integration of Eqs. (54) and (55) with prescribed initial conditions will yield transient solutions. The sign of $\mathrm{d}A/\mathrm{d}\tau$ will change at the value of $A = A^*$ giving the limit-cycle amplitude. Depending on the direction of the change, the stability of the limit cycle is determined. If the derivative is positive (negative) for $A > A^*$ and negative (positive) for $A < A^*$, we have an unstable (stable) limit cycle. In Sec. VI, $\bar{E}_{c,1}$ and $\bar{E}_{s,1}$ are determined for the case of multiple coaxial injection of gaseous propellants.

IV. Solutions for Amplitude and Phase

Let us recast the Eqs. (54) and (55). Define

$$\begin{aligned}
k_1 &\equiv (\gamma-1)\bar{E}_{c,1,\text{excess}};\\
k_2 &\equiv B\left[\frac{\gamma-1}{4\gamma}\frac{\int_0^1(2F_0J_1+F_2J_1)r\,\mathrm{d}r}{\int_0^1J_1^2r\,\mathrm{d}r}+\frac{\gamma^2-1}{32\gamma^2}\frac{\int_0^1J_1^4r\,\mathrm{d}r}{\int_0^1J_1^2r\,\mathrm{d}r}\right]\\
&\quad-\frac{\int_0^1q_{1s}(r)J_1(s_{11}r)r\,\mathrm{d}r}{s_{11}\int_0^1J_1^2(s_{11}r)r\,\mathrm{d}r};\quad k_3 \equiv (\gamma-1)\bar{E}_{s,1};\\
k_4 &\equiv \frac{\int_0^1q_1(r)J_1(s_{11}r)r\,\mathrm{d}r}{s_{11}\int_0^1J_1^2(s_{11}r)r\,\mathrm{d}r} \quad (59)
\end{aligned}$$

Then, Eqs. (54) and (55) become

$$\frac{\mathrm{d}A}{\mathrm{d}\tau} = k_1A+k_2A^3 \quad (60)$$

$$\frac{d\psi}{d\tau} = -2\omega_2 - k_3 - k_4 A^2 \tag{61}$$

The quantities $k_1 A$ and k_3 result from the linear (i.e., first-order) evaluations of the in-phase excess energy release rate and out-of-phase excess energy release rate, respectively. The quantity $k_2 A^3$ ($k_4 A^2$) results from third-order nonlinear in-phase (out-of-phase) contribution from nozzle damping. The parameter k_1 may take either sign depending on whether the combustion driving the contribution exceeds the linear nozzle damping (for $k_1 > 0$) or not (for $k_1 < 0$). It follows from the definition that k_2 is directly proportional to B and, from calculation, is always positive.

Analytical solutions can be found for these two first-order ordinary differential equations. With no loss of generality, take $A = A_0$ and $\psi = 0$ as the initial values. For Eq. (60), separate variables, and recognize that certain differentials of logarithmic terms can be readily constructed. The integrated solution becomes, after some algebraic manipulations,

$$\frac{A(\tau)}{A_0} = \left[\left(1 + \frac{k_2}{k_1}A_0^2\right)e^{-2k_1\tau} - \frac{k_2}{k_1}A_0^2\right]^{-1/2} \tag{62}$$

Consider first the case in which k_1 and k_2 have identical signs, i.e., $k_1 > 0$ and $k_2 > 0$ (Case I). The solution for A goes to infinity in a finite time. Under this condition of unconditional instability in Case I with both k_1 and k_2 having positive values, a stable limit cycle is expected in practice. However, the perturbation series has not yet included sufficiently high powers of ε and A to predict the stable limit cycle. So, the solution is artificially predicted to grow to infinite amplitude in a finite time. Rather, if higher-order analysis were applied, the amplitude solution would be expected to grow to a finite stable amplitude in an infinite time. For example, if an A^5 term with a negative coefficient were added to the right side of Eq. (60), a stable limit cycle could result.

If k_1 and k_2 have opposite signs, a limit cycle clearly exists at $A = A^* \equiv \sqrt{-k_1/k_2}$, where the time derivative becomes zero. For a more informative display, we may rewrite Eq. (62) as

$$\frac{A(\tau)}{A_0} = \left\{\left[1 - \left(\frac{A_0}{A^*}\right)^2\right]e^{-2k_1\tau} + \left(\frac{A_0}{A^*}\right)^2\right\}^{-1/2} \tag{63}$$

If $k_1 < 0$, $k_2 > 0$, and $A_0 < A^*$ (Case IIa), the solution for A decays to zero value as $\tau \to \infty$, while the solution for A grows to infinity in a finite time if $k_1 < 0$, $k_2 > 0$, and $A_0 > A^*$ (Case IIb). (Note that mathematically in either Case IIa or IIb, the value of A^* is approached as $\tau \to -\infty$.) In Case II here, the limit cycle at A^* is unstable. A stable limit cycle should exist at a higher value of $A > A^*$, but the truncated perturbation series does not reveal it. So, again the predicted growth to infinity in a finite time is artificial; rather, growth in an infinite time to a finite stable value is expected. The reversed signs indicate a bistable behavior with conditional stability. Again, if an A^5 term with a negative coefficient were added to the right side of Eq. (60) as a result of higher-order analysis, a stable limit cycle as well as the unstable limit cycle could result.

The frequency perturbation that applies in the limit cycle in which ψ ceases to vary with time is ω_2; thus, its value can be determined from Eq. (61) as a function of A^* to be $\omega_2 = -(k_3 + k_4 A^{*2})/2$. Note that ω_2 can be simply ignored in those cases in which a limit cycle is not found.

Equation (61) is readily solved by integration of a simple quadrature after substitution for A using Eq. (62). The value for ω_2 can be substituted back again into that same equation. In particular, one obtains

$$\begin{aligned}\psi &= -(2\omega_2 + k_3)\tau - k_4\int_0^\tau A^2(\tau')\,d\tau' \\ &= k_4 A^{*2}\tau + \frac{k_4}{2k_2}\ln\left[1 + \frac{k_2}{k_1}A_0^2(1 - e^{2k_1\tau})\right]\end{aligned} \tag{64}$$

Substitution in the argument of the logarithmic function, using Eq. (62), yields

$$\begin{aligned}\psi &= k_4 A^{*2}\tau + \frac{k_4}{2k_2}\ln\left[\left(\frac{A_0}{A}\right)^2 e^{2k_1\tau}\right] \\ &= k_4 A^{*2}\tau - k_4 A^{*2}\tau + \frac{k_4}{2k_2}\ln\left[\left(\frac{A_0}{A}\right)^2\right] = \frac{k_4}{2k_2}\ln\left[\left(\frac{A_0}{A}\right)^2\right]\end{aligned}$$

$$A \to A^* \Rightarrow \psi \to \frac{k_4}{2k_2}\ln\left[\left(\frac{A_0}{A^*}\right)^2\right] \tag{65}$$

V. Comparison with Computational Fluid Dynamics Results

The direct CFD solution of Eqs. (2), (6), and (7) has been performed [11–13]. In unpublished work by Popov et al., results for the postprocessing fitting of that CFD data show that the behavior $d\tilde{A}/d\tilde{t} = C_1\tilde{A} + C_2\tilde{A}^3$ applies in the lower-amplitude region. The coefficient C_1 could be negative or positive, depending on the simulated operational domain. C_2 was always positive. For larger amplitudes, higher-degree polynomials were needed for the fitting. Some qualitative comparison of the results from perturbation theory with the CFD results are useful. For this purpose, we reformulate Eqs. (60) and (61) in dimensional terms in which the dimensional time $\tilde{t} = \frac{R\tau}{a_{ss}\varepsilon^2} = \frac{R\tau}{a_{ss}M}$, the dimensional mean-to-peak pressure amplitude of the major eigenfunction $\tilde{A} = \varepsilon A p_{ss} = \sqrt{M} A p_{ss}$, and the perturbed dimensional frequency of the limit cycle $\tilde{\omega} = \frac{a_{ss}\varepsilon^2\omega_2}{R} = \frac{a_{ss}M\omega_2}{R}$. Now,

$$\frac{d\tilde{A}}{d\tilde{t}} = \frac{Ma_{ss}k_1}{R}\tilde{A} + \frac{k_2 a_{ss}}{p_{ss}^2 R}\tilde{A}^3 \tag{66}$$

and

$$\frac{d\psi}{d\tilde{t}} = -2\tilde{\omega} - \frac{Ma_{ss}k_3}{R} - \frac{k_4 a_{ss}}{p_{ss}^2 R}\tilde{A}^2 \tag{67}$$

Mk_1 and Mk_3 can be written as

$$\begin{aligned}Mk_1 &\equiv M(\gamma - 1)\bar{E}_{c,1,\text{excess}} = (\gamma - 1)\frac{V_3}{2}\left(\sum_{i=1}^{N} A_i\right) - B \\ Mk_3 &\equiv M(\gamma - 1)\bar{E}_{s,1} = \frac{V_4}{2}\left(\sum_{i=1}^{N} A_i\right)\end{aligned} \tag{68}$$

The direct CFD solution of Eqs. (2), (6), and (7) has been performed [11–13]. In unpublished work, results for the postprocessing fitting of that CFD data with the behavior $d\tilde{A}/d\tilde{t} = C_1\tilde{A} + C_2\tilde{A}^3$ have been obtained for certain cases. The coefficient C_1 could be negative or positive, depending on the operational domain. C_2 was always positive.

The multiplication of cos mx or sin mx with cos nx or sin nx where m and n are positive, nonzero integers gives products of the form $\cos(m-n)x$, $\sin(m-n)x$, $\cos(m+n)x$, and $\sin(m+n)x$. Recognition of this pattern leads to the expectation that higher-order (beyond third order) perturbation analysis would yield the generalized relations $d\tilde{A}/d\tilde{t} = \Sigma_{n=1}^{N} C_n \tilde{A}^{2n-1}$ and $d\psi/dt = \Sigma_{n=1}^{N} K_n \tilde{A}^{2n-2}$. One could attempt to match the computational data using a differential equation that has a higher-order polynomial on the right side than the third-degree polynomial of Eq. (66). The generalized relation can be rewritten as $d\tilde{A}^2/d\tilde{t} = 2\Sigma_{n=1}^{N} C_n(\tilde{A}^2)^n$. Thus, the limit-cycle amplitude is given as the solution of $\Sigma_{n=1}^{N} C_n(\tilde{A}^2)^{n-1} = 0$. In Eq. (66), with only two terms, only one solution for $\tilde{A}^2$ can be found, explaining why both a stable limit cycle and an unstable limit cycle were not obtained. With three or more terms on the right side of the generalized version of Eq. (66), it becomes possible to find more solutions and determine both limit cycles.

In the form of Eqs. (66) and (67), the limit-cycle amplitude $\tilde{A}^*$ and frequency modification $\tilde{\omega}^*$ are determined when the derivatives becomes zero; thus,

$$\tilde{A}^* = p_{ss}\sqrt{-\frac{Mk_1}{k_2}}; \qquad \tilde{\omega}^* = \frac{Mk_1k_4a_{ss}}{2k_2R} - \frac{Ma_{ss}k_3}{2R} \tag{69}$$

This result predicts that the limit-cycle mean-to-peak dimensional pressure amplitude $\tilde{A}$ scales roughly as $p_{ss}\sqrt{M}$. However, there are additional Mach-number dependencies from k_1 and k_2; see the definitions of k_1 and k_2 in Eq. (59). The Mach number at the nozzle entrance scales roughly as throat area A_t for a small Mach number ($M \ll 1$), while the steady-state chamber pressure scales as the reciprocal of A_t [24]. Therefore, one should be able to vary A_t at constant mass flow and show that $\tilde{A} \propto A_t^{-1/2}$. Thereby, for example, a 100% increase in the nozzle throat area produces a nearly 30% decrease in the dimensional mean-to-peak limit-cycle amplitude but a 40% increase in the nondimensional amplitude. According to Eq. (69), the frequency perturbation at the limit cycle $\tilde{\omega}^*$ should vary with M (or A_t).

The method here addresses a common case in which the waveform consists of a basic resonant mode of oscillation with the superposition of a fundamental mode described by linear theory and the harmonics of that mode. Although we used the travelling first tangential mode, the method could be used for other tangential modes, radial modes, and mixed radial–tangential modes, including both standing and travelling modes. Situations in which more than one fundamental mode appear with noninteger frequency ratios become more difficult to treat but can be treated by a generalization of the approach here. These situations would produce "wobbly" waveforms for which the solutions cannot be expressed in terms of a single frequency. Energy transfer between these fundamental resonant modes would occur, and subharmonics might be produced.

VI. Integration of Chamber Dynamics and *N* Coaxial Jet Flames

The model for an oscillating coaxial jet turbulent diffusion flame developed by Sirignano and Krieg [27] will be used to describe the mass burning rate and, accordingly, the rate of energy release per unit volume. Only the salient results of that theory are given here; the reader can pursue details in the reference. The steady-state fuel-mass-burning rate associated with the injector is given as

$$\bar{\dot{m}} = 2\pi\bar{D}\frac{p_{ss}}{R_s}\int_0^{L_f}\frac{R_f(x)V_1(x)}{\bar{T}_f(x)}\,dx \tag{70}$$

The total chamber steady-state fuel-mass-burning rate with N identical injectors is $N\bar{\dot{m}}$. The total mass flow rate for injection at the stoichiometric mass ratio is $[(\nu+1)/\nu]N\bar{\dot{m}}$. However, no assumption about the overall mixture ratio has been made. Rich or lean flows can be analyzed. The integrated fuel-mass-burning-rate perturbation for the injector depends on both the instantaneous pressure perturbation and the pressure perturbation at the time of injection for each discrete element of mass. Namely,

$$\dot{m}'(t) = \frac{\gamma-1}{\gamma}\frac{p'(t)}{p_{ss}}\int_0^{L_f}\frac{d\bar{\dot{m}}}{dx}\left[1-\frac{T_{ss,\infty}}{\bar{T}_f(x)}\right]dx - \frac{\gamma-1}{\gamma}\left[\frac{T_{i0}}{T_{ss,\infty}}-1\right]\int_0^{L_f}\frac{T_{ss,\infty}}{\bar{T}_f(x)}\frac{p'(t-x/\bar{U})}{p_{ss}}\frac{d\bar{\dot{m}}}{dx}V_2(x)\,dx \tag{71}$$

The downstream distance for the coaxial jet flame is x. The functions $V_1(x)$ and $V_2(x)$, the flame radial position $R_f(x)$, and the flame temperature $T_f(x)$ are reported by Sirignano and Krieg [27].

The individual injectors experience different pressure histories, depending on their locations. We assume the same design for each injector. Thus, the steady-state mass burning rate, flame temperature, and flame length do not vary from one injector stream to another stream.

Now, to be consistent with the wave dynamics perturbation analysis, the results for the oscillating burning rate should be cast in nondimensional terms. For an injector location centered at the nondimensional position r_i, θ_i with $i = 1, 2, 3, \ldots N$, the pressure terms in Eq. (71) become

$$\begin{aligned}\frac{p'(t,r_i,\theta_i)}{p_{ss}} &= \varepsilon A J_1(s_{11}r_i)\cos(z-\theta_i+\psi)\\ \frac{p'(t-x/\bar{U},r_i,\theta_i)}{p_{ss}} &= \varepsilon A J_1(s_{11}r_i)\cos(z-s_{11}x/\bar{U}-\theta_i+\psi)\\ &= \varepsilon A J_1(s_{11}r_i)[\cos(s_{11}x/\bar{U})\cos(z-\theta_i+\psi)\\ &\quad+\sin(s_{11}x/\bar{U})\sin(z-\theta_i+\psi)]\end{aligned} \tag{72}$$

where x and $\bar{U}$ are now normalized using the chamber radius R and the steady-state sound speed a_{ss}.

The perturbation of the energy release rate is obtained as follows. Define the steady-state energy rate as $\bar{E} = Q\bar{\dot{m}}$ and the energy-rate perturbation for the individual injector as $E_{i'} = Q\dot{m}'$, where Q is the fuel-heating value. Normalize these energy rates by the quantity $p_{ss}a_{ss}R^2$. Substitute Eq. (72) into Eq. (71), multiply by Q, and perform the normalization to yield an expression for E_i'. At the scale of the chamber wave dynamics, the burning rate is taken as a delta function at the point r_i, θ_i, namely, $\delta(r-r_i, \theta-\theta_i)$. The perturbation of the nondimensional energy release rate for the ith injector becomes

$$\begin{aligned}E_i'(z,r_i,\theta_i) &= \frac{\gamma-1}{\gamma}\varepsilon A J_1(s_{11}r_i)\delta(r-r_i,\theta-\theta_i)\\ &\times\left\{\cos(z-\theta_i+\psi)\left[\int_0^{L_f}\frac{d\bar{E}}{dx}\left(1-\frac{T_{ss,\infty}}{\bar{T}_f(x)}\right)dx\right.\right.\\ &\left.+\left(1-\frac{T_{i0}}{T_{ss,\infty}}\right)\int_0^{L_f}\frac{T_{ss,\infty}}{\bar{T}_f(x)}\cos(s_{11}x/\bar{U})\frac{d\bar{E}}{dx}V_2(x)\,dx\right]\\ &+\sin(z-\theta_i+\psi)\left(1-\frac{T_{i0}}{T_{ss,\infty}}\right)\\ &\left.\times\int_0^{L_f}\frac{T_{ss,\infty}}{\bar{T}_f(x)}\sin(s_{11}x/\bar{U})\frac{d\bar{E}}{dx}V_2(x)\,dx\right\}\\ &= \varepsilon A J_1(s_{11}r_i)\delta(r-r_i,\theta-\theta_i)[V_3\cos(z-\theta_i+\psi)\\ &+V_4\sin(z-\theta_i+\psi)]\end{aligned} \tag{73}$$

where x and L_f are normalized by R and the definitions for V_3 and V_4 are

$$\begin{aligned}V_3 &\equiv \frac{\gamma-1}{\gamma}\left[\int_0^{L_f}\frac{d\bar{E}}{dx}\left(1-\frac{T_{ss,\infty}}{\bar{T}_f(x)}\right)dx\right.\\ &\left.+\left(1-\frac{T_{i0}}{T_{ss,\infty}}\right)\int_0^{L_f}\frac{T_{ss,\infty}}{\bar{T}_f(x)}\cos(s_{11}x/\bar{U})\frac{d\bar{E}}{dx}V_2(x)\,dx\right\}\\ V_4 &\equiv \frac{\gamma-1}{\gamma}\left(1-\frac{T_{i0}}{T_{ss,\infty}}\right)\int_0^{L_f}\frac{T_{ss,\infty}}{\bar{T}_f(x)}\sin(s_{11}x/\bar{U})\frac{d\bar{E}}{dx}V_2(x)\,dx\end{aligned} \tag{74}$$

The two integrals in Eq. (74) with the sinusoidal and cosinusoidal functions of $s_{11}x/\bar{U}$ (i.e., kinematic waveforms) in the integrand can be expected to be small because the short kinematic wavelength leads to substantial cancellation in the integration over the flame length L_f. Comparison among Eqs. (21), (73), and (74) gives support to the assumption made earlier that $|\bar{E}_{c,1}| \gg |\bar{E}_{s,1}|$.

If the pressure fluctuation at the injector and the energy-release-rate fluctuation of the jet flame are described, respectively, by $p' = Pe^{i\omega t}$ and $E' = E_1e^{i\omega t}$, then the nondimensional linear response coefficient can be constructed for an individual injector as a complex number using the imaginary unit i by taking the ratio of E' and p',

$$\frac{E'}{p'} = \frac{E_1}{P} = V_3 - iV_4 \tag{75}$$

This complex quantity is named the combustion response factor; it provides information about the in-phase response of the energy

release rate to a pressure fluctuation through V_3 and the out-of-phase response of the energy release rate to a pressure fluctuation through V_4. The combustion response factor is commonly expressed in complex notation for linear analyses, but that form is not very useful for a nonlinear analysis. Since the physical interest is in the real part of the number, squares and products of the complex numbers are not relevant. Thus, complex notation is avoided here, and instead the in-phase V_3 and out-of-phase V_4 components are each addressed separately.

The total energy-release-rate perturbation is determined by summing the contribution of the N individual injectors from Eq. (73), which yields

$$E' = \Sigma_{i=1}^{N} E_i'(z, r_i, \theta) \tag{76}$$

Now, the right side of Eq. (76) will be expanded in an eigenfunction series using products of Bessel functions of the first kind and first order (i.e., J_1) and their corresponding sinusoidal and cosinusoidal functions. For convenience, use the identities $\cos(z - \theta_i + \psi) = \cos(z + \psi)\cos\theta_i + \sin(z + \psi)\sin\theta_i$ and $\sin(z - \theta_i + \psi) = \sin(z + \psi)\cos\theta_i - \cos(z + \psi)\sin\theta_i$. Some convenient definitions are

$$\begin{aligned}
a_i &\equiv \frac{\int_0^{2\pi}\int_0^1 \delta(r - r_i, \theta - \theta_i) J_1(s_{11} r_i)\cos\theta_i J_1(s_{11} r)\cos\theta r\,\mathrm{d}r\,\mathrm{d}\theta}{\pi \int_0^1 J_1^2(s_{11} r) r\,\mathrm{d}r} \\
&= \frac{J_1^2(s_{11} r_i)\cos^2\theta_i}{\pi \int_0^1 J_1^2(s_{11} r) r\,\mathrm{d}r}; \\
b_i &\equiv \frac{\int_0^{2\pi}\int_0^1 \delta(r - r_i, \theta - \theta_i) J_1(s_{11} r_i)\sin\theta_i J_1(s_{11} r)\sin\theta r\,\mathrm{d}r\,\mathrm{d}\theta}{\pi \int_0^1 J_1^2(s_{11} r) r\,\mathrm{d}r} \\
&= \frac{J_1^2(s_{11} r_i)\sin^2\theta_i}{\pi \int_0^1 J_1^2(s_{11} r) r\,\mathrm{d}r}; \qquad A_i \equiv a_i + b_i = \frac{J_1^2(s_{11} r_i)}{\pi \int_0^1 J_1^2(s_{11} r) r\,\mathrm{d}r}
\end{aligned} \tag{77}$$

Only the lowest-frequency terms in the eigenfunction expansion will be a factor in driving the lowest harmonic of the chamber oscillation and will be kept here. The other terms can influence the higher-order higher frequency harmonics. Those higher-order effects are beyond the current considerations. The leading (i.e., lowest-frequency) terms in the eigenfunction expansion with account for contributions from all N injectors are represented as

$$\begin{aligned}
E_1(z, r, \theta) &= \varepsilon A J_1(s_{11} r)\Bigg[V_3\left(\sum_{i=1}^{N} a_i\right)\cos(z + \psi)\cos\theta \\
&+ V_3\left(\sum_{i=1}^{N} b_i\right)\sin(z + \psi)\sin\theta + V_4\left(\sum_{i=1}^{N} a_i\right)\sin(z + \psi)\cos\theta \\
&- V_4\left(\sum_{i=1}^{N} b_i\right)\cos(z + \psi)\sin\theta\Bigg] \\
&= \varepsilon A J_1(s_{11} r)\Bigg\{\frac{V_3}{2}\left[\sum_{i=1}^{N} A_i\right]\cos(z - \theta + \psi) \\
&+ \frac{V_3}{2}\left[\sum_{i=1}^{N} A_i\cos(2\theta_i)\right]\cos(z + \theta + \psi) \\
&+ \frac{V_4}{2}\left[\sum_{i=1}^{N} A_i\cos(2\theta_i)\right]\sin(z + \theta + \psi) \\
&+ \frac{V_4}{2}\left[\sum_{i=1}^{N} A_i\right]\sin(z - \theta + \psi)\Bigg\} \\
E_1(z, r, \theta) &\approx \varepsilon A J_1(s_{11} r)\Bigg[\frac{V_3}{2}\left(\sum_{i=1}^{N} A_i\right)\cos(z - \theta + \psi) \\
&+ \frac{V_4}{2}\left(\sum_{i=1}^{N} A_i\right)\sin(z - \theta + \psi)\Bigg]
\end{aligned} \tag{78}$$

After integration with the Dirac delta function, $E_1(z, r, \theta)$ is now a measure of the fluctuation in the time rate of energy per unit volume. Equation (78) shows that the burning rate and energy release rate have waveforms travelling in both θ directions. However, the summations in the coefficients for the waves travelling in the negative θ direction have a mixture of positive and negative signs due to the presence of the $\cos(2\theta_i)$ factor. Therefore, the net effect of negative-θ wave travel is diminished, and we need deal only with the dominant positive-θ direction, as indicated by the final approximation in Eq. (78).

Comparison of the coefficients in Eqs. (22) and (24) with Eq. (78) leads to the results

$$\begin{aligned}
&\bar{E}_{c,1} = \frac{V_3}{2}\left(\sum_{i=1}^{N} A_i\right); \qquad \bar{E}_{c,1,\text{excess}} = \frac{1}{M}\left[\frac{V_3}{2}\left(\sum_{i=1}^{N} A_i\right) - \frac{B}{\gamma - 1}\right]; \\
&\bar{E}_{s,1} = \frac{1}{M}\frac{V_4}{2}\left(\sum_{i=1}^{N} A_i\right)
\end{aligned} \tag{79}$$

These results may now be used for substitution in Eqs. (54) and (55).

VII. Results

Results are presented for the specific example with coaxial injectors, demonstrating the matching process between wave dynamics and the injection/combustion mechanisms with N coaxial injectors and associated jet flames. Calculations have been made to analyze the solutions for the amplitude and phase as functions of time using the perturbation theory. The results are obtained using the oscillating coaxial jet turbulent diffusion flame model developed by Sirignano and Krieg [27]. Results are presented here considering methane and gaseous-oxygen propellants with a fuel-to-oxygen mass stoichiometric coefficient of 1/4. The ratio of specific heats $\gamma = 1.3$ and steady-state pressure of 200 atm have been chosen. For all calculations, the quantity $Q/(c_p T_{i0}) = 64.5$ remains constant. A combustion chamber diameter of 0.28 m and chamber length of 0.5 m are considered.

Different cases are considered to gain a representative picture of the possible outcomes. For the base case, the mean flow chamber Mach number is varied, considering a combustion chamber consisting of ten injectors, each with an outer radius of 1.1 cm and inner radius of 0.898 cm. The fuel and oxidizer leave each injector with an axial velocity of 200 m/s. Six of the ten injectors are placed every $\pi/3$ rad at a radial position of $(3/4)R$, three injectors are placed every $2\pi/3$ rad at a radial position of $(1/2)R$, and the last injector is placed at the center of the chamber. This is the same ten-injector setup analyzed and portrayed by Sirignano and Popov [11].

Four different parameter surveys are performed. For Surveys 1–3, the mean flow chamber Mach number is kept fixed at 0.066, and the same ten-injector configuration is analyzed. For Survey 1, the ratio of the outer injector radius to the inner injector radius is kept fixed so that the mixture ratio is the same as in the base case. The magnitudes of the injector radii are varied, keeping the mass flux factor UR_o^2 fixed with the same value as in the base case. For Survey 2, the outer injector radius is kept at 1.1 cm with an axial velocity of 200 m/s. The mixture ratio is varied by changing the inner radius of the injector. For Survey 3, the ratio of the steady-state mean chamber-gas temperature to the initial injection temperature is varied, keeping the same injector radii and axial velocity as in the base case.

For Survey 4, the mean flow chamber Mach number is 0.066, the axial velocity is 200 m/s, and the mixture ratio is the same as in the base case. The number of injectors is varied from 10 to 19, keeping the quantity NR_o^2 fixed, which fixes the total mass flux. Sketches of four selected injector configurations are shown in Fig. 1. The $N = 10$ injector configuration is the base case. Injectors are then added one by one by first adding three injectors to the middle ring at $(1/2)R$ and then adding six additional injectors to the outer ring at $(3/4)R$. The value of R_o is shown to decrease with increasing N in order to control the mass flux.

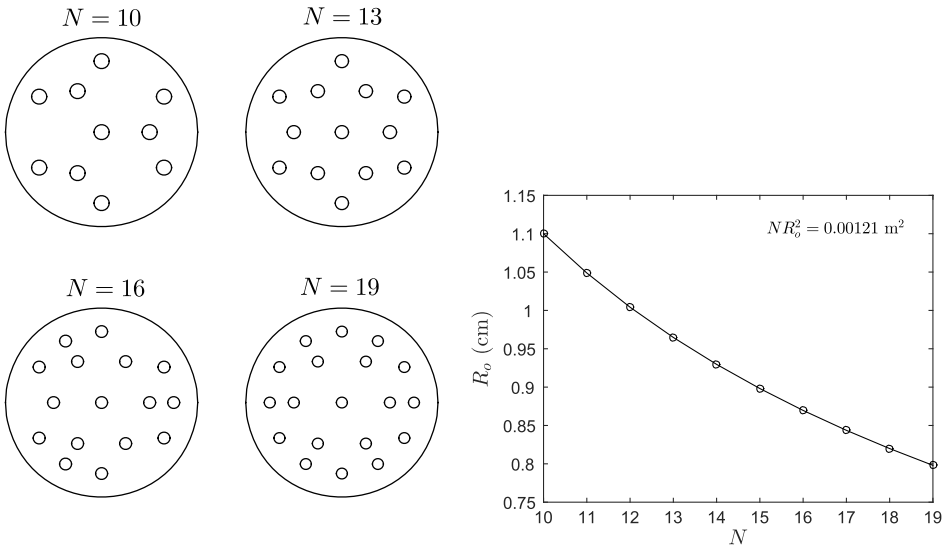

Fig. 1 Injector configurations. The number of injectors N varies between 10 and 19. The outer radius R_o of the injector is adjusted to keep the total mass flux constant.

In Surveys 1 and 4, the mean chamber-gas temperature naturally remains fixed because the mixture ratio is fixed. However, for Survey 2, the constant gas temperature is an artificial constraint; as the mixture becomes more rich, the mean gas temperature should decrease. The practical effect of the mixture ratio change appears through both the injector radii ratio and the gas temperature ratio. For example, as the mixture gets richer, the injector radii ratio increases while gas temperature decreases. Thus, to get the practical effect of the mixture ratio variation, the variations in two parameters should be coupled.

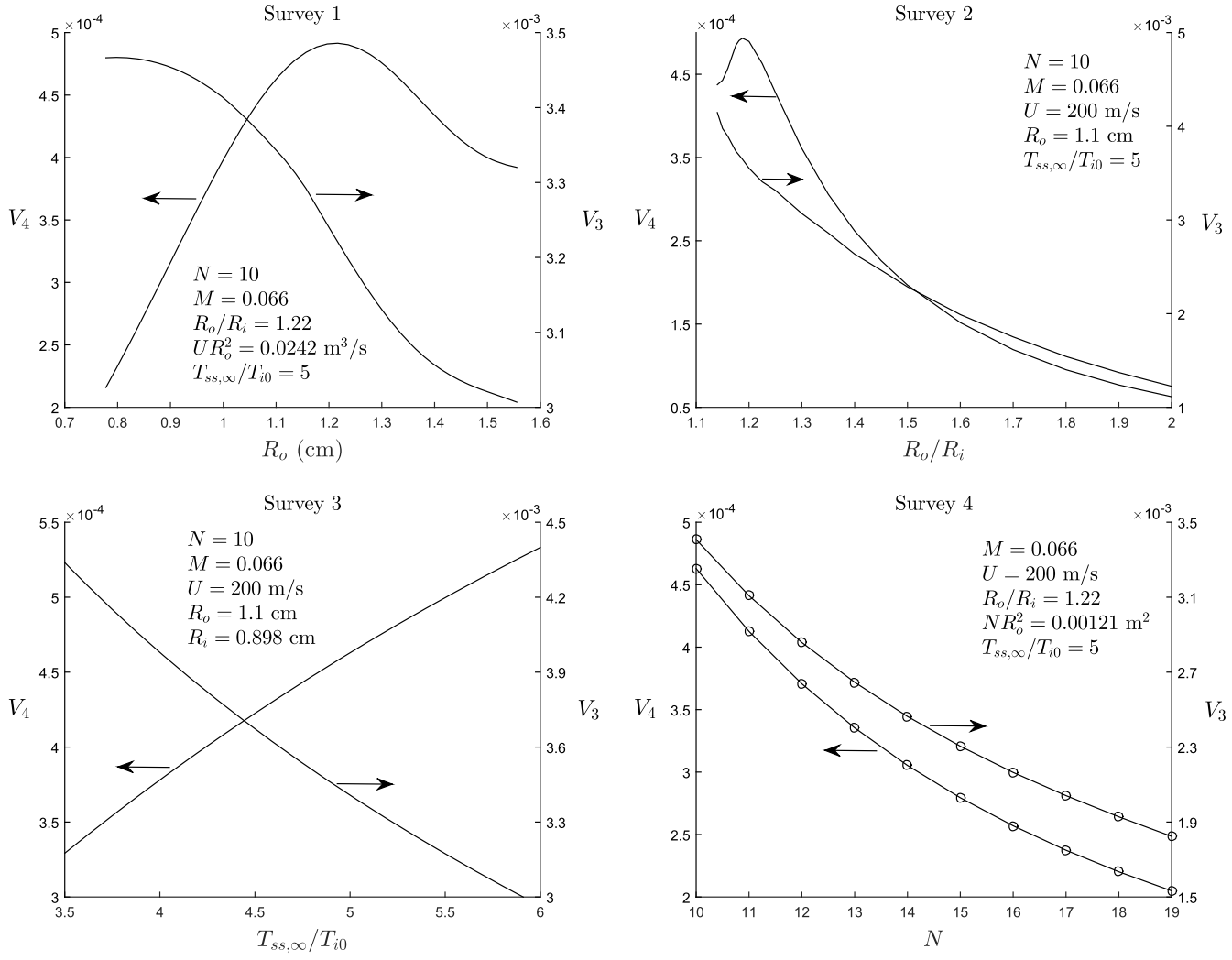

Fig. 2 Variation of V_3 and V_4.

A. Combustion Response Factor

It is necessary to calculate in sequence certain quantities before obtaining results for the amplitude and phase as functions of the slow time variable. Here, we will report the results in an order matching the required sequence. For each of the different cases, the quantities V_3 and V_4 are calculated, which relate the energy release rate to a pressure fluctuation, giving both the in-phase and out-of-phase components, as shown by Eq. (73). The results are presented in Fig. 2 for all surveys. Both V_3 and V_4 are independent of Mach number, so the values for the base case are constant, with $V_3 = 3.407 \times 10^{-3}$ and $V_4 = 4.629 \times 10^{-4}$.

The results in Fig. 2 show that the in-phase component of the combustion response factor decreases as R_o increases. Basically, this the Strouhal number effect [27]. Namely, the mixing time increases as

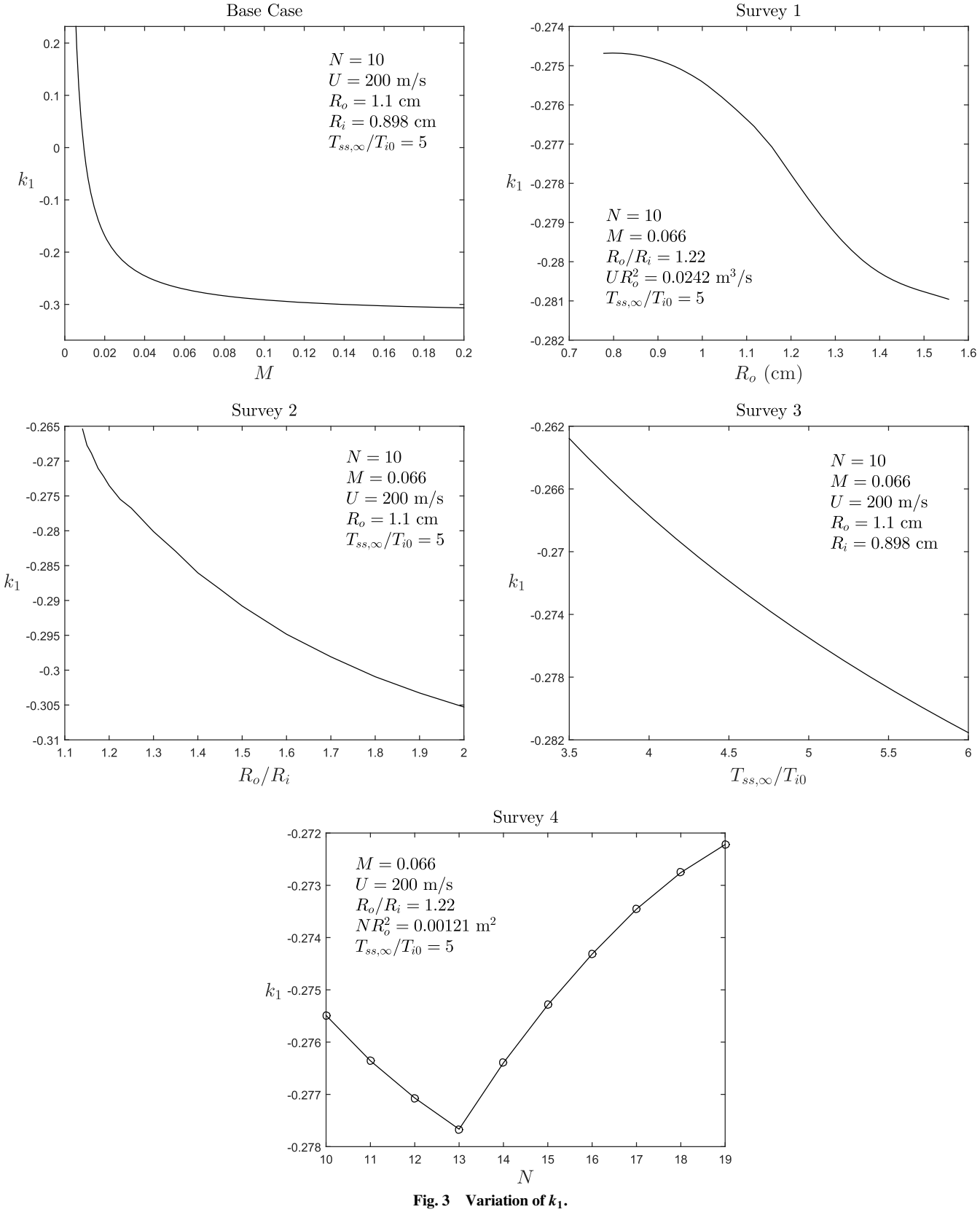

Fig. 3 Variation of k_1.

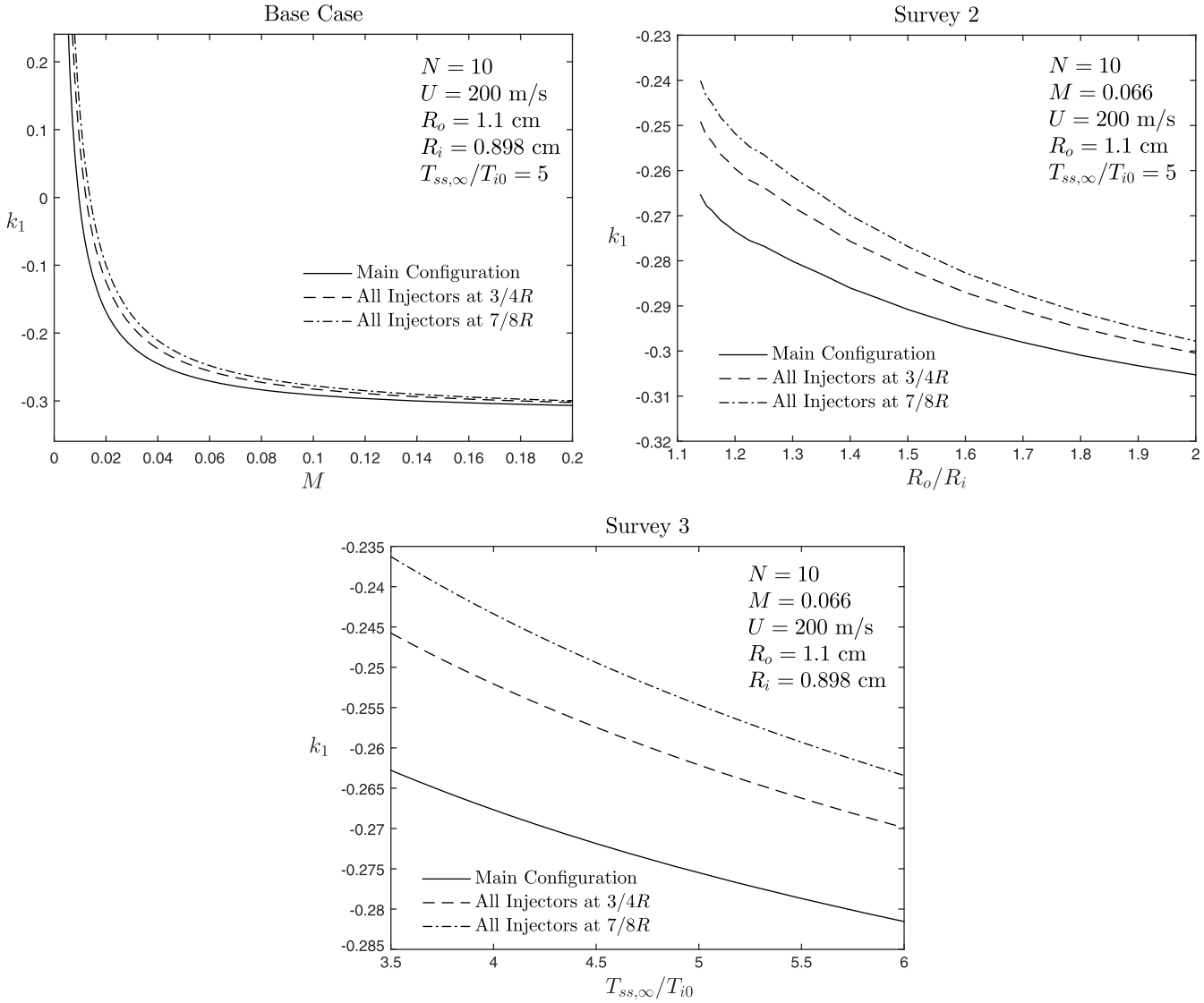

Fig. 4 The effect on k_1 of moving the injectors outward.

the radius increases and the mismatch between the period of oscillation and the mixing time increases. As R_o/R_i increases, the mixture becomes more fuel rich and thereby less energetic, causing a decrease of the in-phase response factor. The increase in the inflow temperature T_{i0} causes a higher flame temperature and thereby a greater value of the in-phase combustion response. Since V_3 and V_4 are representative of an individual injector stream, their values decrease as the number of injectors are increased at constant total mass flow; each injector has decreased mass flow and becomes less energetic as more injectors are added.

B. Constants for Amplitude and Phase Dynamics

Once the values for V_3 and V_4 are known, the energy release coefficients are readily determined after integration (i.e., connection) with the injection configuration. The coefficients, k_1 through k_4 are determined following Eq. (59). Also, k_1 and k_3 in the perturbation solution need information about the combustion process through Eq. (79), after multiplying by a factor containing the ratio of specific heats of the mixture. The coefficient k_1 depends on the balance between the linear combustion driving mechanism and the linear nozzle damping mechanism. The coefficient k_2 is derived from the nonlinear interaction of the nozzle with the wave dynamics and does not depend on the coaxial flame model. The term k_2A^3 is a nonlinear correction to k_1A in Eq. (60). A positive value of k_2 means that the nonlinear correction to nozzle damping reduces the damping from the overprediction of the linear theory. The k_4 value is determined from the nonlinear wave dynamics alone without any effects from the combustion or the nozzle. In particular, for our first tangential mode

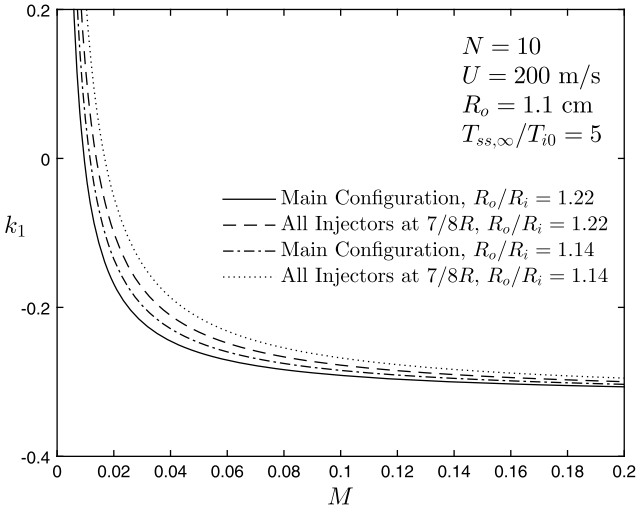

Fig. 5 The effect on k_1 of moving the injectors outward, comparing the base case with a leaner mixture at a fixed temperature ratio.

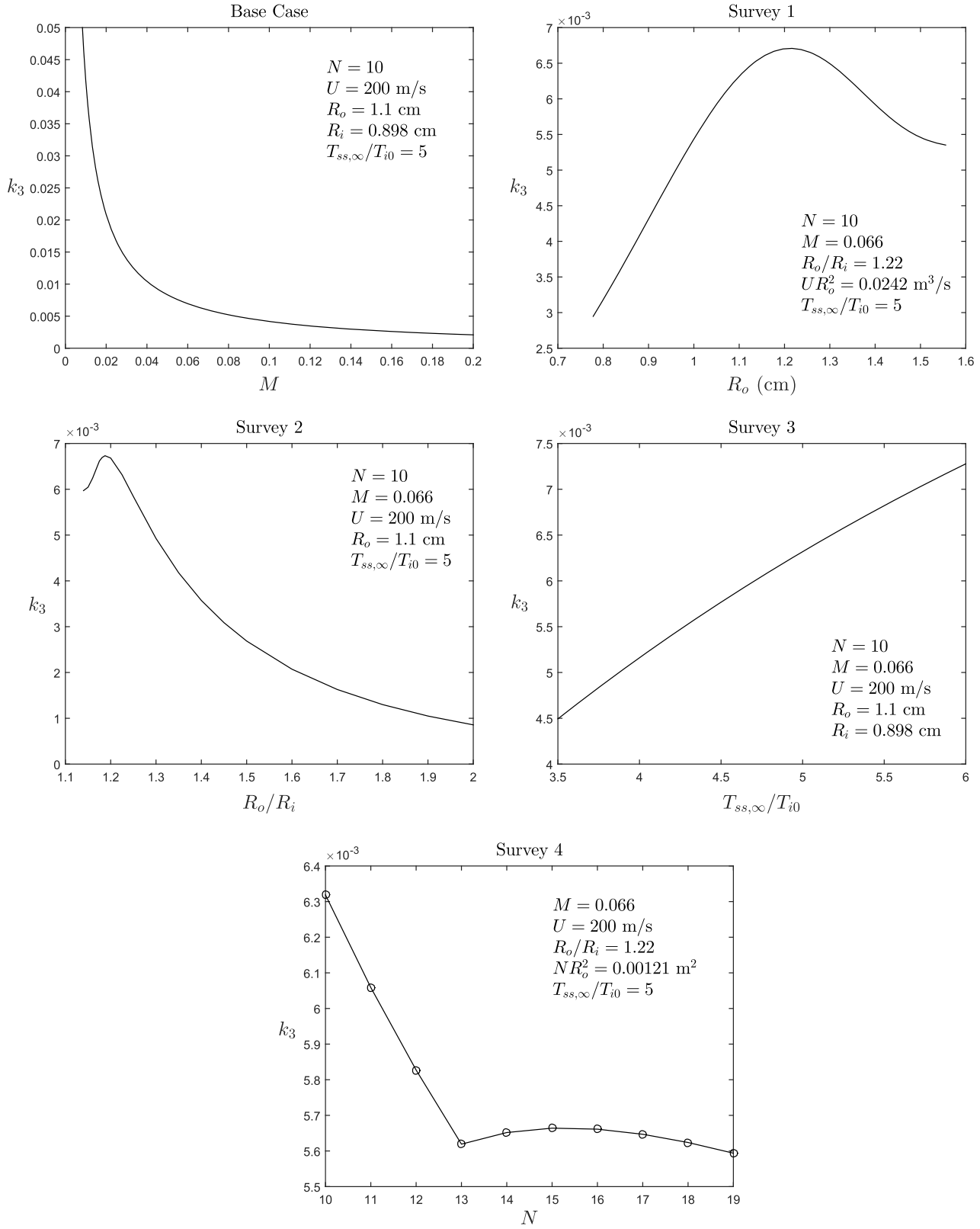

Fig. 6 Variation of k_3.

with the value $\gamma = 1.3$, we have $k_2 = 2.2699M$ and $k_4 = 1.5318$. Thus, k_2 depends only on M, while k_4 is independent of the surveyed parameters.

Special attention is given first to k_1, which is critical for both linear and nonlinear stability behavior. The variation of the coefficient k_1 for the overall study is given in Fig. 3. It follows closely the behavior of V_3.

The variation in Mach number has the most significant effect on the value of k_1. For very small Mach numbers less than about 0.012, the value for k_1 is positive and increases exponentially as the Mach number decreases toward zero. In this region, the model predicts unconditional instability. As the Mach number increases, the coefficient k_1 approaches a constant value. For Survey 1, when the Mach number, mixture ratio, and mass flux are fixed, an increase in

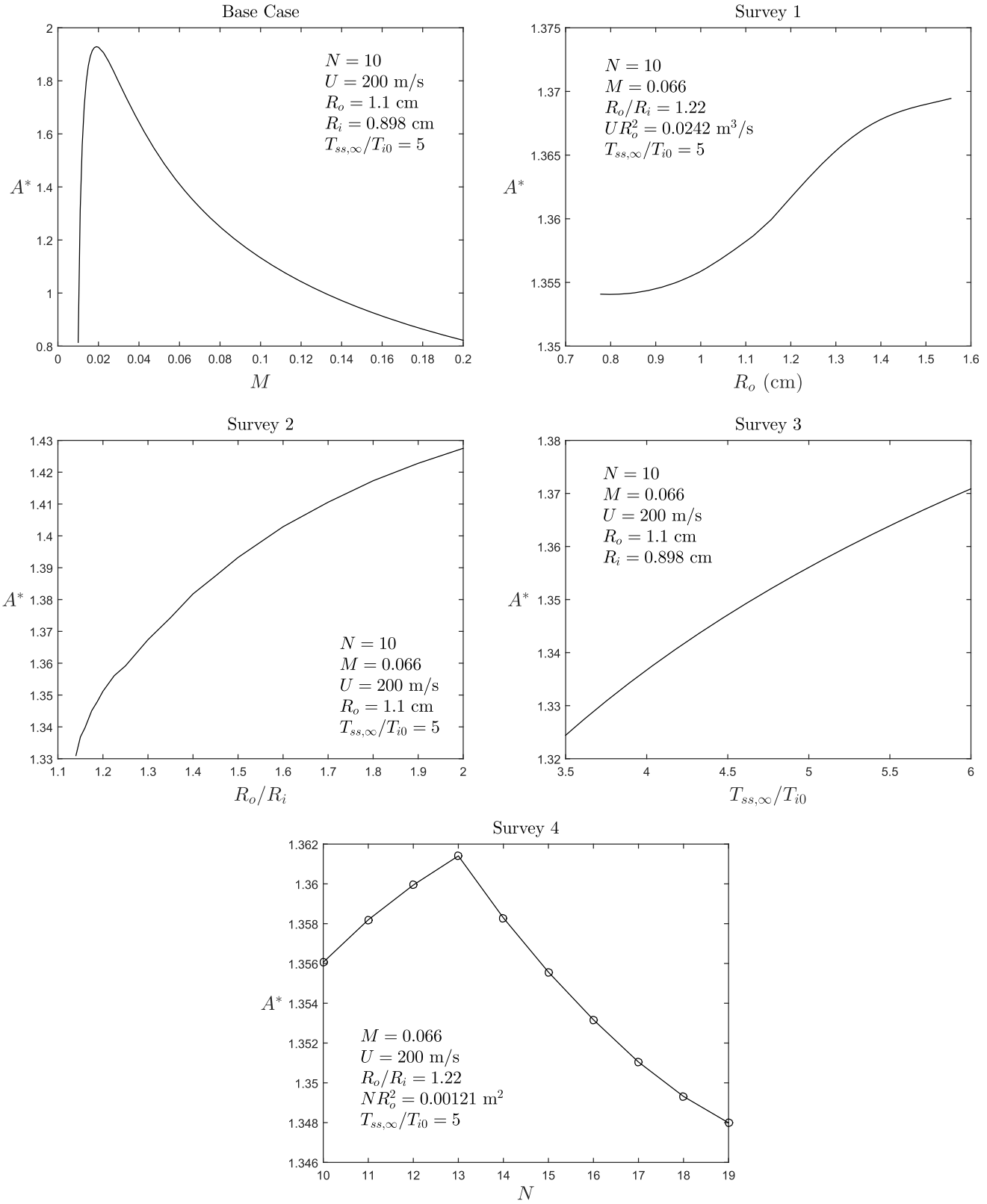

Fig. 7 Variation of limit-cycle amplitude A^*.

the injector radii causes k_1 to decrease slightly. Again, this can be described as a Strouhal number effect caused by the relation between the jet mixing time and the oscillation period. For the specific values considered here, k_1 decreases by only about 3% across the entire domain. For Survey 2, it is seen that less rich or near-stoichiometric mixtures have a higher (i.e., less negative) value of k_1 than fuel-rich mixtures. For Survey 3, k_1 decreases in an approximately linear fashion as the temperature ratio $T_{\mathrm{ss},\infty}/T_{i0}$ increases. For Survey 4, as three injectors are added one by one at a radial position of $(1/2)R$, the value of k_1 decreases; however, as additional injectors are added at $(3/4)R$, k_1 increases. Nonetheless, the value of k_1 only changes by about 2% when the number of injectors is increased from 13 to 19.

As shown in Fig. 3, it is predicted that, for a given Mach number, the value of k_1 may be increased by moving injectors outward in radial position, by changing the mixture ratio to produce a leaner mixture, or by decreasing the temperature ratio $T_{\mathrm{ss},\infty}/T_{i0}$. Additional

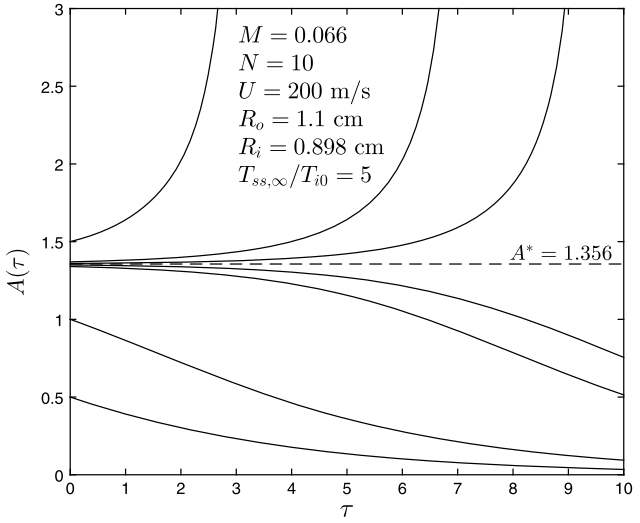

Fig. 8 Amplitude solution $A(\tau)$ for the base case.

cases are examined to gain a more representative picture of the operating conditions in which k_1 becomes positive, indicating unconditional instability. Figure 4 shows the variation of k_1 vs the Mach number when the injectors are moved from the main configuration described previously to a configuration in which all ten injectors are located at a radial position of either $(3/4)R$ or $(7/8)R$. The pressure amplitude increases with the radial position, meaning that the energy-release-rate oscillation, which increases with the pressure amplitude, also increases with the radial position. Therefore, more energy is added to the oscillation as the radial positions of the injector and flame are increased, making the configuration more unstable. Figure 4 also shows the effect on k_1 for different mixture ratios and temperature ratios when the injectors are moved outward. Figure 5 compares the distribution of k_1 vs the Mach number for two different mixture ratios: the base case ($R_o = 1.1$ cm and $R_i = 0.898$ cm) and the most fuel-lean case. By using a less rich mixture and moving the injectors outward to $(7/8)R$, the critical Mach number indicting the onset of instability increases by nearly a factor of 2.

The behavior of k_3 shown in Fig. 6 follows closely the behavior of V_4 shown in Fig. 2. In particular, similar monotonic trends with the temperature ratio are seen, and peak values occur as R_o or R_o/R_i vary. Interestingly, the behavior as more injectors are added is not quite monotonic. The behavior with M is expected from the definition of k_3.

C. Amplitude: Transient Behavior and Triggering Threshold

The signs for k_1 and k_2 affect the stability of the system. For a positive k_2, there are two different scenarios predicted. For positive k_2 and positive k_1, the solution is unconditionally unstable, and the amplitude A goes to infinity in a finite time. For positive k_2 and negative k_1, a limit cycle exists, in which the solution will decay below a certain critical amplitude and grow to infinity above the critical amplitude. Of course, growth to an infinite amplitude should not occur if higher-order terms were included in the perturbation series. In a linear analysis, only k_1 without k_2 would appear; in the framework of the linear world, positive (negative) k_1 means that any perturbation, no matter how small (large), would grow (decay).

The limit-cycle amplitude A^* is determined from the values of k_1 and k_2 for the different cases. Since k_2 is always positive, the limit-cycle amplitude only exists for regions where k_1 is negative. In that case, the limit cycle is unstable and becomes the triggering threshold. Thus, the larger (smaller) the value of A^*, the more stable (unstable) the configuration in nonlinear terms. The results are presented in Fig. 7. The nondimensional limit-cycle amplitude varies most significantly with the Mach number. The maximum limit-cycle amplitude is reached near a Mach number of 0.02. In the region where $k_1 < 0$, the magnitudes of both k_1 and k_2 are monotonically increasing functions of M. Since the slope of the k_1 magnitude decreases with M while the k_2 slope is constant, the ratio produces a maximum. For Survey 1, increasing the injector radii at a constant mixture ratio increases that amplitude slightly. For Survey 2, the more fuel-rich mixtures have a modestly larger limit-cycle amplitude than the lean mixtures. For Survey 3, the limit-cycle amplitude increases slightly as the temperature ratio $T_{ss,\infty}/T_{i0}$ increases. For Survey 4, the amplitude increases as the three injectors are added one by one to the middle ring but decreases as additional injectors are added to the outer ring.

Figure 8 gives the solution for the amplitude as a function of the slow time τ for the base case at a chamber-mean-flow Mach number of 0.066. The unstable-limit-cycle amplitude $A^* = 1.356$ has been determined from the values of k_1 and k_2 at the corresponding Mach number. For an initial amplitude greater than A^*, the solution goes to infinity in a finite time; for an initial amplitude less than A^*, the amplitude gradually decays to zero. This behavior is representative of the scenarios in which $k_1 < 0$ and $k_2 > 0$. For very small Mach numbers with positive k_1, a limit cycle does not exist, and the solution goes to infinity unconditionally, regardless of the initial amplitude.

Of course, it is not expected that the amplitude should ever grow to infinity. In the case in which an unstable limit cycle exists, we expect the existence of a stable limit cycle of greater amplitude. For the case of linear instability (unconditional instability), we also expect a stable limit cycle to occur. A higher-order expansion of our perturbation series would introduce additional nonlinear damping and should predict the stable limit cycle.

For the base case at a mean-flow Mach number of 0.066, results are compared to those presented by Sirignano and Popov [11] for the coupled coaxial-injector and combustion-chamber-wave-dynamics models. For the ten-injector design configuration, imposing a first tangential mode as the initial condition, Sirignano and Popov [11] show the existence of nonlinear triggering corresponding to an unstable limit cycle of approximately 20 atm. For initial amplitudes below 20 atm, the oscillation decays. For initial amplitudes above 20 atm, the oscillation amplitude grows toward a stable limit cycle at 155 atm. Qualitatively, the present perturbation theory also predicts an unstable limit cycle for the same operating conditions and injector configuration. Higher-order perturbation analysis would be required in order to predict the presence of a higher-amplitude stable limit cycle. For the perturbation theory, the corresponding pressure amplitude Δp (atm) for the unstable limit cycle is evaluated at the chamber wall and is given by $\Delta p = \sqrt{M}A^*J_1(s_{11})p_{ss}$. For the base case at $M = 0.066$, the pressure oscillation amplitude is 40 atm, twice the value calculated by Sirignano and Popov [11]. There are several possible explanations for the differences. The CFD result includes the effects of all harmonics in the waveform, while the amplitude reported now for the perturbation calculation addresses only the fundamental component. Second, the amplitude that is reported here for the fundamental component of the first tangential mode applies only to the contribution that appeared from the $O(\varepsilon)$ solution; that fundamental frequency behavior can also appear from higher-order results as a homogeneous solution to the higher-order separated partial differential equations.

D. Nonlinear Frequency Correction

The two coefficients k_3 and k_4 determine the transient change in phase through Eq. (55) and ultimately determine the frequency for the limit cycle. The results for the nonlinear frequency correction ω_2 are presented in Fig. 9. Except for the dependence on M, the variations with parameters are modest.

VIII. Conclusions

A perturbation analysis for first-tangential-mode combustion instability in a liquid-propellant rocket engine has been developed through third order in the perturbation parameter using a two-time-variable method that yields information not obtained by previous perturbation expansions for combustion-chamber oscillations. The method allows determinations of the transient growth or decay of the oscillation, the threshold for the triggering of the instability in the

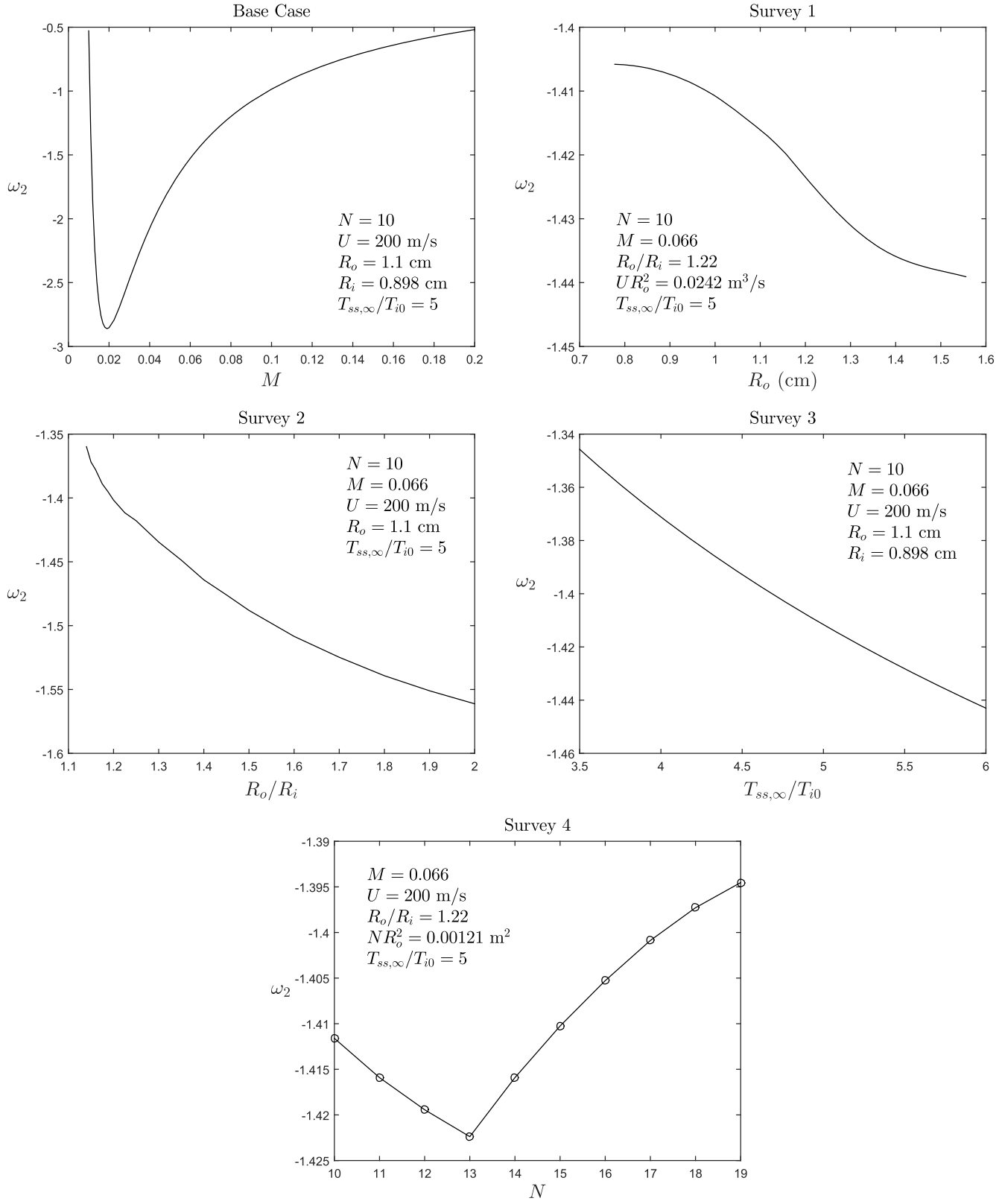

Fig. 9 Variation of frequency perturbation ω_2.

bistable domain, the variation of the phase with time, and the nonlinear correction to the frequency. For the first time, the proper perturbation parameter has been identified as the square root of the mean-flow Mach number in the combustion chamber. Development of the expansion to third order is necessary and sufficient to obtain these results. To second and third orders, higher harmonics with nonresonant frequencies are superimposed on the oscillation. The amplitude and phase of the oscillation vary with the slow time as described by a system of two first-order ordinary differential equations. The amplitude variation with time has an exact solution, and the particular amplitude of the unstable limit cycle (when one exists) is predicted. Unconditionally unstable and conditionally stable domains in the space of operational parameters are predicted.

For the operating domain considered here, the stable limit cycle is not predicted by the series truncated at third order. There is reason to believe that a higher-order expansion would yield the stable limit cycle for cases of unconditional instability (the linearly unstable regime) and conditional stability (the nonlinearly unstable regime). Furthermore, it should predict cases of unconditional stability.

Stability characteristics, e.g., growth and decay rates and triggering threshold (i.e., unstable-limit-cycle amplitude), are predicted as functions of the mean-flow Mach number; number, size, and locations of injectors; mixture ratio; and steady-state to initial-injection temperature ratio. As the mixture becomes more fuel rich or as the propellant inflow temperature is reduced, the engine becomes more stable. Moving a higher fraction of the propellant flow away from the chamber center has a destabilizing effect on the tangential mode. The trend with the varying Mach number is not monotonic; a most stable value of M is deduced. The trends predicted for changes in operational parameters are consistent with prior CFD results. For example, the threshold for triggering is predicted within a factor of 2. The proportionality of the amplitude parameter with the square root of the mean-flow Mach number M for the tangential oscillation contrasts with earlier results [2,10] for the longitudinal mode that gives the amplitude parameter proportional to M. The longitudinal-mode perturbation analysis with the shock formation forces a balancing between damping and driving terms at second order, while the tangential mode brings the balance at third order. This explains why tangential oscillations are found to have much higher amplitudes than the longitudinal waves.

This two-time-variable perturbation method is valuable for predicting trends and qualitative behavior because it is less costly than a CFD analysis. It also has value in identifying the critical physics in the balance between those phenomena driving the oscillation and those phenomena damping it. A simple system of two first-order ordinary differential equations that provides a basis for future active-control studies is produced.

Appendix: Definitions and Derivative Evaluations

The $q_n(r)$ and $Q_n(r)$ values are given in the following. Unless noted otherwise, the arguments of the Bessel functions are $s_{11}r$, and nondimensional variables are used,

$$q_0(r) \equiv \frac{1}{\gamma r^2}[(J_2^2 - J_1^2)(2 - s_{11}^2 r^2) + s_{11} r J_1 J_2]$$
$$Q_0(r) \equiv \frac{1}{\gamma}[(J_1^2 - J_2^2)(2 - s_{11}^2 r^2) - s_{11} r J_1 J_2] \tag{A1}$$

$$\begin{aligned} q_1 \equiv{}& \frac{\gamma-1}{\gamma}\left[\frac{J_1 Q_0}{r^2} + \frac{J_1 Q_2}{2r^2} - s_{11}^2 J_1 F_0 - \frac{s_{11}^2 J_1 F_2}{2} + \frac{3 s_{11}^2 J_1^3}{8\gamma} - \frac{s_{11}^2 J_1^3}{4}\right] - \frac{2}{s_{11}}\left\{\left(\frac{J_1}{r} - s_{11} J_2\right)\frac{\mathrm{d}^2 G_2}{\mathrm{d}r^2} + \left[s_{11}^2(J_3 - J_1) - \frac{4 s_{11} J_2}{r} + \frac{2 J_1}{r^2}\right]\frac{\mathrm{d}G_2}{\mathrm{d}r}\right. \\ &\left. + \left[\frac{3 s_{11} J_2}{r^2} - \frac{s_{11}^2}{r}(3J_1 + J_3) + s_{11}^3 J_2\right] G_2\right\} + \frac{1}{s_{11} r}\left[\frac{s_{11} J_2 G_2}{r} - \frac{J_1}{r}\frac{\mathrm{d}G_2}{\mathrm{d}r} + s_{11}^2 J_1 H_2 - \left(2\frac{J_1}{r} - s_{11} J_2\right)\frac{\mathrm{d}H_2}{\mathrm{d}r} - \frac{J_1 H_2}{r^2}\right] \\ &+ \frac{\gamma-1}{\gamma^2 s_{11} r}\left[\frac{2 s_{11} J_1 (J_2^2 - J_1^2)}{r} - 2\left(\frac{J_1}{r}\right)^2 J_2 + \frac{s_{11}^2}{2} J_1^2 J_2 + \frac{s_{11}^3 r}{2} J_1 (J_1^2 - J_2^2) - \frac{1}{4 s_{11}}\left(\frac{J_1}{r}\right)^3 + \frac{3}{2 s_{11}} J_2 \left(\frac{J_1}{r}\right)^2\right] \\ &+ \frac{1}{2\gamma^2 s_{11} r}\left[2 s_{11} J_2 \left(\frac{J_1}{r}\right)^2 - \frac{11 s_{11}^2}{2}\frac{J_1^3}{r} + 2 s_{11}^2 J_2^2 \frac{J_1}{r} - \frac{7 s_{11}^3}{2} J_2^3 + 6 s_{11}^3 J_1^2 J_2 + s_{11}^4 r J_1^3 - \frac{7 s_{11}^4 r}{2} J_1 J_2^2\right] \end{aligned} \tag{A2}$$

$$\begin{aligned} q_{1s} \equiv{}& \frac{\gamma-1}{\gamma}\left[\frac{J_1 Q_{2s}}{2r^2} + \frac{3 s_{11}^2 J_1 F_{2s}}{2}\right] + \frac{1}{\gamma s_{11}^2}\left\{\left(\frac{J_1}{r} - s_{11} J_2\right)\frac{\mathrm{d}^3 F_{2s}}{\mathrm{d}r^3} + \left[s_{11}^2(J_3 - J_1) - \frac{4 s_{11} J_2}{r} + \frac{2 J_1}{r^2}\right]\frac{\mathrm{d}^2 F_{2s}}{\mathrm{d}r^2}\right. \\ &\left. + \left[\frac{3 s_{11} J_2}{r^2} - \frac{s_{11}^2}{r}(3J_1 + J_3) + s_{11}^3 J_2\right]\frac{\mathrm{d}F_{2s}}{\mathrm{d}r}\right\} + \frac{1}{s_{11} r}\left[\frac{J_1}{r}\frac{\mathrm{d}G_{2s}}{\mathrm{d}r} - \frac{s_{11} J_2 G_{2s}}{r} + s_{11}^2 J_1 H_{2s} - \left(\frac{2 J_1}{r} - s_{11} J_2\right)\frac{\mathrm{d}H_{2s}}{\mathrm{d}r} - \frac{J_1 H_{2s}}{r^2}\right] \end{aligned} \tag{A3}$$

$$q_2(r) \equiv -s_{11}^2 J_1^2 + \frac{s_{11}^2}{\gamma} J_2^2 - \frac{s_{11} J_1 J_2}{\gamma r};$$
$$Q_2(r) \equiv s_{11}^2 r^2 J_1^2 - \frac{s_{11}^2 r^2}{\gamma} J_2^2 + \frac{s_{11} r J_1 J_2}{\gamma} \tag{A4}$$

$$q_{2s}(r) \equiv B s_{11}\left[2F_2 + \frac{\gamma-1}{4\gamma} J_1^2\right];$$
$$Q_{2s}(r) \equiv -B s_{11} r^2\left[2F_2(r) + \frac{\gamma-1}{4\gamma} J_1^2\right] \tag{A5}$$

$$
\begin{aligned}
q_3 \equiv{}& \frac{\gamma-1}{\gamma}\left[\frac{J_1 Q_2}{2r^2}-\frac{9s_{11}^2 J_1 F_2}{2}+\frac{s_{11}^2 J_1^3}{8\gamma}+\frac{s_{11}^2 J_1^3}{4}\right]\\
&+\frac{2}{s_{11}}\left\{\left(\frac{J_1}{r}-s_{11}J_2\right)\frac{\mathrm{d}^2G_2}{\mathrm{d}r^2}+\left[s_{11}^2(J_3-J_1)-\frac{4s_{11}J_2}{r}+\frac{2J_1}{r^2}\right]\frac{\mathrm{d}G_2}{\mathrm{d}r}+\left[\frac{3s_{11}J_2}{r^2}-\frac{s_{11}^2}{r}(3J_1+J_3)+s_{11}^3J_2\right]G_2\right\}\\
&+\frac{1}{s_{11}r}\left[\frac{s_{11}J_2(3G_2+4H_2)}{r}-\frac{3J_1}{r}\frac{\mathrm{d}G_2}{\mathrm{d}r}-3s_{11}^2J_1H_2+\left(2\frac{J_1}{r}-3s_{11}J_2\right)\frac{\mathrm{d}H_2}{\mathrm{d}r}-\frac{J_1H_2}{r^2}\right]\\
&+\frac{\gamma-1}{\gamma^2 s_{11}r}\left[2s_{11}\left(\frac{J_1}{r}\right)^3-\frac{s_{11}^2}{2}J_1^2J_2+s_{11}^3rJ_1(J_2^2-J_1^2)-\frac{3}{4s_{11}}\left(\frac{J_1}{r}\right)^3+\frac{1}{2s_{11}}J_2\left(\frac{J_1}{r}\right)^2\right]\\
&+\frac{1}{2\gamma^2 s_{11}r}\left[-8s_{11}J_2\left(\frac{J_1}{r}\right)^2+\frac{3s_{11}^2}{2}\frac{J_1^3}{r}+6s_{11}^2J_2^2\frac{J_1}{r}+\frac{9s_{11}^3}{2}J_2^3-6s_{11}^3J_1^2J_2-s_{11}^4rJ_1^3+\frac{7s_{11}^4r}{2}J_1J_2^2\right];\\
q_{3s} \equiv{}& \frac{\gamma-1}{\gamma}\left[\frac{J_1 Q_{2s}}{2r^2}-\frac{13s_{11}^2 J_1 F_{2s}}{2}\right]\\
&-\frac{1}{\gamma s_{11}^2}\left\{\left[\frac{J_1}{r}-s_{11}J_2\right]\frac{\mathrm{d}^3F_{2s}}{\mathrm{d}r^3}+\left[s_{11}^2(J_3-J_1)-\frac{4s_{11}J_2}{r}+\frac{2J_1}{r^2}\right]\frac{\mathrm{d}^2F_{2s}}{\mathrm{d}r^2}+\left[\frac{3s_{11}J_2}{r^2}-\frac{s_{11}^2}{r}(3J_1+J_3)+s_{11}^3J_2\right]\frac{\mathrm{d}F_{2s}}{\mathrm{d}r}\right\}\\
&+\frac{1}{s_{11}r}\left[\frac{3J_1}{r}\frac{\mathrm{d}G_{2s}}{\mathrm{d}r}+\frac{s_{11}J_2(4H_{2s}-3G_{2s})}{r}-3s_{11}^2J_1H_{2s}+\left(\frac{2J_1}{r}-3s_{11}J_2\right)\frac{\mathrm{d}H_{2s}}{\mathrm{d}r}-\frac{J_1H_{2s}}{r^2}\right]
\end{aligned}
\tag{A6}
$$

It is convenient to use the relations

$$
\begin{aligned}
&\frac{\mathrm{d}F_2}{\mathrm{d}r}=4\pi s_{11}^2\left\{\left[\frac{Y_2(2s_{11}r)}{r}-s_{11}Y_3(2s_{11}r)\right]\int_0^r\frac{J_2(2s_{11}r')Q_2(r')}{r'}\mathrm{d}r'-\left[\frac{J_2(2s_{11}r)}{r}-s_{11}J_3(2s_{11}r)\right]\int_0^r\frac{Y_2(2s_{11}r')Q_2(r')}{r'}\mathrm{d}r'\right\};\\
&\frac{\mathrm{d}F_{2s}}{\mathrm{d}r}=4\pi s_{11}^2\left\{\left[\frac{Y_2(2s_{11}r)}{r}-s_{11}Y_3(2s_{11}r)\right]\int_0^r\frac{J_2(2s_{11}r')Q_{2s}(r')}{r'}\mathrm{d}r'-\left[\frac{J_2(2s_{11}r)}{r}-s_{11}J_3(2s_{11}r)\right]\int_0^r\frac{Y_2(2s_{11}r')Q_{2s}(r')}{r'}\mathrm{d}r'\right\};\\
&\frac{\mathrm{d}^2F_2}{\mathrm{d}r^2}=\frac{Q_2}{r^2}+\frac{4F_2}{r^2}-4s_{11}^2F_2-\frac{1}{r}\frac{\mathrm{d}F_2}{\mathrm{d}r};\quad \frac{\mathrm{d}^3F_2}{\mathrm{d}r^3}=\frac{1}{r^2}\frac{\mathrm{d}Q_2}{\mathrm{d}r}-\frac{3Q_2}{r^3}+(4s_{11}^2r^2-12)\frac{F_2}{r^3}+\left(\frac{6}{r^2}-4s_{11}^2\right)\frac{\mathrm{d}F_2}{\mathrm{d}r};\\
&\frac{\mathrm{d}^2F_{2s}}{\mathrm{d}r^2}=\frac{Q_{2s}}{r^2}+\frac{4F_{2s}}{r^2}-4s_{11}^2F_{2s}-\frac{1}{r}\frac{\mathrm{d}F_{2s}}{\mathrm{d}r};\quad \frac{\mathrm{d}^3F_2}{\mathrm{d}r^3}=\frac{1}{r^2}\frac{\mathrm{d}Q_{2s}}{\mathrm{d}r}-\frac{3Q_{2s}}{r^3}+(4s_{11}^2r^2-12)\frac{F_{2s}}{r^3}+\left(\frac{6}{r^2}-4s_{11}^2\right)\frac{\mathrm{d}F_{2s}}{\mathrm{d}r};\\
&\frac{\mathrm{d}G_2}{\mathrm{d}r}=\frac{1}{2\gamma^2s_{11}^2}\left[\frac{J_1J_2}{r^3}-\frac{5s_{11}J_2^2}{2r^2}-\frac{s_{11}J_1J_3}{r^2}+\frac{s_{11}^2J_2J_3}{r}-\gamma s_{11}\frac{\mathrm{d}^2F_2}{\mathrm{d}r^2}\right];\quad \frac{\mathrm{d}G_{2s}}{\mathrm{d}r}=\frac{1}{2\gamma s_{11}}\frac{\mathrm{d}^2F_{2s}}{\mathrm{d}r^2};\\
&\frac{\mathrm{d}^2G_2}{\mathrm{d}r^2}=\frac{1}{2\gamma^2s_{11}^2}\left[-4\frac{J_1J_2}{r^4}-\frac{3s_{11}J_1J_3}{r}-\frac{s_{11}^2J_1J_2}{r^2}+9\frac{s_{11}^2J_2J_3}{r^2}-\frac{s_{11}^3J_3^2}{r}+\frac{s_{11}^2J_1J_4}{r^2}-\frac{s_{11}^3J_2J_4}{r}-\gamma s_{11}\frac{\mathrm{d}^3F_2}{\mathrm{d}r^3}\right];\quad \frac{\mathrm{d}^2G_{2s}}{\mathrm{d}r^2}=\frac{1}{2\gamma s_{11}}\frac{\mathrm{d}^3F_{2s}}{\mathrm{d}r^3};\\
&\frac{\mathrm{d}H_2}{\mathrm{d}r}=\frac{1}{\gamma s_{11}r}\left[\frac{\mathrm{d}F_2}{\mathrm{d}r}-\frac{F_2}{r}+\frac{J_1^2+J_2^2}{4\gamma r}-\frac{s_{11}J_1J_2}{2\gamma}+\frac{J_1J_2}{2\gamma s_{11}r^2}-\frac{s_{11}J_2J_3}{2\gamma}-\frac{J_1J_3}{2\gamma r}\right];\quad \frac{\mathrm{d}H_{2s}}{\mathrm{d}r}=\frac{1}{\gamma s_{11}r}\left[\frac{\mathrm{d}F_{2s}}{\mathrm{d}r}-\frac{F_{2s}}{r}\right]
\end{aligned}
\tag{A7}
$$

Acknowledgments

This research was supported by the Air Force Office of Scientific Research under grants FA9550-12-1-0156 and FA9550-15-1-0033 with Mitat Birkan as the Program Manager.

References

[1] Harrje, D., and Reardon, F., "Liquid Propellant Rocket Combustion Instability," NASA SP-194, 1972.

[2] Sirignano, W. A., "Driving Mechanisms for Combustion Instability," *Combustion Science and Technology*, Vol. 187, Nos. 1–2, 2015, pp. 162–205. doi:10.1080/00102202.2014.973801

[3] Oefelein, J. C., and Yang, V., "Comprehensive Review of Liquid-Propellant Combustion Instabilities in F-1 Engines," *Journal of Propulsion and Power*, Vol. 9, No. 5, 1993, pp. 657–677. doi:10.2514/3.23674

[4] Crocco, L., and Cheng, S.-I., *Theory of Combustion Instability in Liquid Propellant Rocket Motors, AGARD Monograph 8*, Butterworths, London, 1956.

[5] Reardon, F. H., Crocco, L., and Harrje, D. T., "Velocity Effects in Transverse Mode Liquid Propellant Rocket Combustion Instability," *AIAA Journal*, Vol. 2, No. 9, 1964, pp. 1631–1641. doi:10.2514/3.2631

[6] Culick, F. E. C., *Unsteady Motions in Combustion Chambers for Propulsion Systems*, North Atlantic Treaty Organization, AGARDograph AG-AVT-039, Neuilly-Sur-Seine, France, 2006.

[7] Minorsky, N., *Nonlinear Oscillations*, Van Nostrand, Princeton, NJ, 1962, pp. 462–487.

[8] Sirignano, W. A., "Theoretical Study of Nonlinear Combustion Instability: Longitudinal Mode," Ph.D. Dissertation, Report No. 677, Dept. of Aerospace and Mechanical Sciences, Princeton Univ., Princeton, NJ, March 1964.

[9] Zinn, B. T., "A Theoretical Study of Nonlinear Combustion Instability in Liquid-Propellant Rocket Engines," *AIAA Journal*, Vol. 6, No. 10, 1968, pp. 1966–1972. doi:10.2514/3.4908

[10] Sirignano, W. A., and Crocco, L., "A Shock Wave Model of Unstable Rocket Combustors," *AIAA Journal*, Vol. 2, No. 7, 1964, pp. 1285–1296. doi:10.2514/3.2534

[11] Sirignano, W. A., and Popov, P. P., "Two-Dimensional Model for Liquid-Rocket Transverse Combustion Instability," *AIAA Journal*,

Vol. 51, No. 12, 2013, pp. 2919–2934.
doi:10.2514/1.J052512
[12] Popov, P. P., Sideris, A., and Sirignano, W. A., "Stochastic Modelling of Transverse Wave Instability in a Liquid-Propellant Rocket Engine," *Journal of Fluid Mechanics*, Vol. 745, April 2014, pp. 62–91.
doi:10.1017/jfm.2014.96
[13] Popov, P. P., Sirignano, W. A., and Sideris, A., "Propellant Injector Influence on Liquid-Propellant Rocket Engine Instability," *Journal of Propulsion and Power*, Vol. 31, No. 1, 2015, pp. 320–331.
doi:10.2514/1.B35400
[14] Popov, P. P., Sideris, A., and Sirignano, W. A., "Triggering and Re-Stabilization of Combustion Instability with Rocket Motor Acceleration," *AIAA Journal* (to be published).
[15] Popov, P. P., and Sirignano, W. A., "Transverse Combustion Instability in a Rectangular Rocket Motor," *Journal of Propulsion and Power.*
doi:10.2514/1.B35868
[16] Mitchell, C. E., Crocco, L., and Sirignano, W. A., "Nonlinear Longitudinal Instability in Rocket Motors with Concentrated Combustion," *Combustion Science and Technology*, Vol. 1, No. 1, 1969, pp. 35–64.
doi:10.1080/00102206908952190
[17] Crocco, L., and Mitchell, C. E., "Nonlinear Periodic Oscillations in Rocket Motors with Distributed Combustion," *Combustion Science and Technology*, Vol. 1, No. 2, 1969, pp. 146–169.
doi:10.1080/00102206908952197
[18] Sirignano, W. A., "A Theory of Axial-Mode Shock-wave Oscillations in a Solid-Rocket Combustor," *Twelfth Symposium (International) on Combustion*, Combustion Inst., Pittsburgh, PA, 1968, pp. 129–37.
[19] Awad, E., and Culick, F., "On the Existence and Stability of Limit Cycles for Longitudinal Acoustic Modes in a Combustion Chambers," *Combustion Science and Technology*, Vol. 46, Nos. 3–6, 1986, pp. 195–222.
doi:10.1080/00102208608959800
[20] Yang, V., and Culick, F., "On the Existence and stability of Limit Cycles for Transverse Acoustic Oscillations in a Cylindrical Combustion Chamber: I Standing Modes," *Combustion Science and Technology*, Vol. 72, Nos. 1–3, 1990, pp. 37–65.
doi:10.1080/00102209008951639
[21] Yang, V., Kim, S., and Culick, F., "Triggering of Longitudinal Pressure Oscillations Combustion Chambers: I Nonlinear Gas Dynamics," *Combustion Science and Technology*, Vol. 72, Nos. 4–6, 1990, pp. 183–214.
doi:10.1080/00102209008951647
[22] Yang, V., and Anderson, W. (ed.), *Liquid Rocket Engine Combustion Instability*, Vol. 169, Progress in Astronautics and Aeronautics, AIAA, Washington, D.C., 1995.
[23] Crocco, L., and Sirignano, W. A., "Behavior of Supercritical Nozzle Under Three Dimensional Oscillatory Conditions," North Atlantic Treaty Organization AGARDograph No. 117, Neuilly-Sur-Seine, France, 1967.
[24] Crocco, L., and Sirignano, W. A., "Effect of the Transverse Velocity Component on the Nonlinear Behavior of Short Nozzles," *AIAA Journal*, Vol. 4, No. 8, 1966, pp. 1428–1430.
doi:10.2514/3.3691
[25] Kevorkian, J. K., and Cole, J. D., *Multiple Scale and Singular Perturbation Methods (Applied Mathematical Sciences)*, Springer–Verlag, New York, 1996, pp. 267–386.
[26] Abramowitz, M., and Stegun, I. A., *Handbook of Mathematical Functions*, Dover, New York, 1965, p. 360.
[27] Sirignano, W. A., and Krieg, J., "Co-Axial Jet Flame Subject to Long-Wavelength Acoustic Oscillations," *Journal of Propulsion and Power.*
doi:10.2514/1.B35953

J. C. Oefelein
Associate Editor